Albite Feldspar Mineral Raman and ATR-IR Fingerprints obtained with q-Gaussian and q-BWF deconvolutions made by means of Fityk Software

Sparavigna, Amelia Carolina[1]

This work is proposing the fingerprints of Raman and ATR-IR spectra of feldspar Albite minerals. The Raman fingerprints are based on q-Gaussian functions deconvolution, whereas the ATR-IR fingerprints are obtained with q- Gaussian and q-BWF functions deconvolutions. q-Gaussian and q-BWF functions are implemented in Fityk software. Literature about albite and its use in glasses and ceramics is also provided.

Notes

Supplementary material

https://data.mendeley.com/datasets/74b2fw4fw4/1

Keywords and subjects

Raman spectroscopy | ATR-IR spectroscopy | Albite | q-Gaussian functions | q-BWF functions

Details

DOI
DOI 10.5281/zenodo.14743007

Resource type
Working paper

Publisher
Zenodo

Citation

Sparavigna, A. C. (2025). Albite Feldspar Mineral Raman and ATR-IR Fingerprints obtained with q-Gaussian and q-BWF deconvolutions made by means of Fityk Software. Zenodo. https://doi.org/10.5281/zenodo.14743007

Albite Feldspar Mineral Raman and ATR-IR Fingerprints obtained with q-Gaussian and q-BWF deconvolutions made by means of Fityk Software

Amelia Carolina Sparavigna

Department of Applied Science and Technology, Polytechnic University of Turin, Turin, Italy

Torino, 23 January 2025, amelia.sparavigna@polito.it

Abstract: This work is proposing the fingerprints of Raman and ATR-IR spectra of feldspar Albite minerals. The Raman fingerprints are based on q-Gaussian functions deconvolution, whereas the ATR-IR fingerprints are obtained with q-Gaussian and q-BWF functions deconvolutions. q-Gaussian and q-BWF functions are implemented in Fityk software. Literature about albite and its use in glasses and ceramics is also provided.

The first use of the term "fingerprint" in relation to the Raman spectroscopy seems to be in an article published in 1947 about the Raman spectra of hydrocarbons by Fenske and coworkers. Fenske et al., 1947, wrote that the bands of the Raman spectrum, "which are called Raman lines, are characteristic of the substance illuminated and are therefore a "fingerprint" of that substance". From that time on, the points of identification, such as positions of peaks, shoulders and valleys create the characteristic spectral pattern which is known as the "Raman fingerprint" of a given material. This pattern allows the material classification, "without any preliminary information about composition and structural origin of the individual features" (D'Ippolito et al., 2015).

Besides Raman spectra, we can consider the 'fingerprints' also of ATR-IR spectra. Here we determine both Raman and ATR-IR fingerprints for ***feldspar Albite minerals***. Data are kindly provided by the ***RRUFF database*** (Lafuente et al., 2015). We discussed the Raman and Attenuated Total Reflectance Infrared RRUFF spectra in Sparavigna, 2024.

The deconvolution of the Raman spectra (depolarized) is proposed determined by means of q-Gaussian functions. Deconvolutions are obtained using Fityk software (Wojdyr, 2010). The centers of the peaks and the parameters of the components are given in files .peaks by Fityk. The q-Gaussians are defined by Sparavigna in a script for this software. The deconvolution of the ATR-IR spectra is obtained with both q-BWF and q-Gaussian functions; in this case too, the functions are defined by Sparavigna with a script in Fityk. The q-Breit-Wigner-Fano function is an asymmetric form of the q-Gaussian function.

The mineral

Albite is a feldspar mineral. It is the sodium endmember of the corresponding mineral group, with ideal formula $NaAlSi_3O_8$. Anorthite is the calcium endmember of the same group. Albite and anorthite spectra are given by https://rruff.info/tags=54. We can find also in the group of alkali feldspars, the "K-end member ($KAlSi_3O_8$, orthoclase and microcline)" (Fuentes et al., 2022).

In Wikipedia, it is said that two variants of albite exist: the 'low albite' and 'high albite'. Both variants are triclinic, but they are different in the unit cell volume, that is larger in the case of the 'high' form. The 'high' form can be produced from the 'low' form by heating above 750 °C (1,380 °F) (Wikipedia, mentioning Tuttle and Bowen, 1950). "The crystal structure of low albite, Amelia, Virginia, was determined at l3 K by neutron diffraction" (Smith et al., 1986).
Fuertes et al., 2018, illustrate the two forms as follows: "Albite may be found with an ordered or disordered structure. The ordered structure is known as low albite, which belongs to the triclinic pinacoidal crystal system. Its framework consists of rings of four tetrahedron, where each tetrahedron is centered by a Si^{4+} or an Al^{3+}. Each oxygen atom is located at the corners of the tetrahedron and links two tetrahedron which are usually labeled as T1o, T1m, T2o and T2m. The completely disorder triclinic albite is known as high albite. Disordered albite undergoes a triclinic to monoclinic phase transition at about 980 °C, where the complete order is lost. In that case, albite framework is formed by two tetrahedral sites, i.e T1 and T2" (Fuertes et al., 2018, and references therein).
"Albite is used as a gemstone, albeit semiprecious. Albite is also used by geologists as it is identified as an important rock forming mineral. There is some industrial use for the mineral such as the manufacture of glass and ceramics" (Wikipedia).
For the Aluminosilicate Glasses, "Adding aluminum oxide to basic soda lime glasses increases the durability of the glass and opens the choices for raw material selection. Aluminosilicate glasses are useful at higher temperatures and have greater thermal shock resistance. Resistance to weathering, water, and chemicals is excellent, although acid resistance is only fair when compared with other glasses. Alumina may be obtained by the addition of albite ($NaAlSi_3O_8$) in the form of feldspar or nepheline syenite" (Mooney, 1996).
Regarding ceramics, "Previous studies about the dielectric behavior and the conduction mechanism of feldspars at high temperature and high pressure showed an insulator behavior and suggested an ionic conduction as the dominant conduction mechanism" (Fuertes et al., 2018). Fuertes and coworkers propose "A novel glass-ceramic material based on albite type Na-rich feldspar has been synthesized by conventional ceramic process". The dielectric properties they determined "make this novel material a very promising candidate in the market of ceramic electrical insulator, highlighting for high-voltage applications" (Fuertes et al., 2018).
In 2022, Fuertes and coworkers stress that "The unique compositional and structural features as well as the many outstanding properties that feldspars own, make them to be widely used as raw material for the ceramic industry. Moreover, multiple works have demonstrated that engineered feldspar-based ceramics are very promising for their use in applications such as ceramic tiles, dielectrics or phosphors, among others". Fuentes et al., 2022, are providing "a comprehensive review on their dielectric, mechanical, optical and thermal properties".

Albite in Italy

Albitites are granular dike rocks consisting essentially of albite.
"Albitites are unique metasomatic rocks formed by the action of sodium-rich fluids on granitoids and/or acid metamorphics. Such an albitization process can lead to a high degree of replacement of albite after plagioclase and K-feldspar. Albitites represent the major source of fluxes for the ceramic tile industry with over 9 million tons per year from about 70 active sites. The largest deposits are located in the Menderes massif in southwestern Turkey, where several mines are in operation. Further active mining districts are in central Sardinia, Italy, and eastern Pyrenées, France" (Dondi et al., 2019, and references therein). Regarding the "mineral resources for the

ceramic industry", a "survey of feldspathic raw materials in Italy" is proposed by Dondi et al., 2025. "The ceramic industry manufactures a diverse array of products … which rely on feldspathic fluxes as fundamental ingredients. These fluxes are crucial for providing the appropriate amount of liquid phase during firing, which is necessary for viscous flow sintering. It is estimated that the production of these vitrified ceramics consumes between 300 and 400 million tons of raw materials annually, with a significant portion consisting of feldspathic fluxes" (Dondi et al., 2025, ands references therein).

In Palomba, 2001, it is stressed that "Albitite is considered a valuable raw material for the ceramic industry, chiefly as flux materials for ceramic tiles, once-fired white tiles and unglazed stoneware " (Palomba, 2001, mentioning Bornioli et al., 1996). "The largest albitite occurrences in Europe, mined for albite, are located in Central Sardinia, at the Southern margin of the Tirso river rift valley, where the Hercynian granitoid massif extensively crops out. The parent rocks of the albitites are … . The main mineralogical association of albitites consists of rarely zoned plagioclase and quartz. Subordinate minerals are K-feldspar, biotite, chlorite, epidote, titanite, and muscovite" (Palomba, 2001). Albite has been found at the Somma-Vesuvio volcano too (Russo et al., 2007).

Literature about spectroscopy of Albite

In McKeown, 2005, the Raman spectra "for crystalline albite from 25 °C to above the 1118 °C melting temperature" have been proposed. The vibrational assignments were made by means of lattice dynamics. "The 25 °C calculations determined that localized T-O stretch and O-T-O bend modes are above 900 cm^{-1} (where T = Si,Al), while motions from the aluminosilicate tetrahedral cage mixed with Na displacements occur in modes as high as 814 cm^{-1}. Vibrational modes for the most prominent peaks in the spectrum, between 350 and 550 cm^{-1}, are dominated by four-membered tetrahedral ring deformations. For completeness, calculated infrared mode frequencies and their atomic displacements are reported for the 25 °C structure and compared with normal mode calculation results and observed infrared mode frequencies presented by von Stengel (1977)" (McKeown, 2005).

"The assignments [based on McKeown's (2005) calculations for low albite] show that the two strongest Raman bands in the 450–520 cm^{-1} spectral region (Group I) belong to the ring-breathing modes of the four-membered rings of tetrahedra. The Raman peaks in Groups II and III (below 400 cm^{-1}) correspond to rotation-translation modes of the four-membered rings and cage-shear modes, respectively. The weaker Raman peaks in the 900–1200 cm^{-1} region (Group V) were assigned to the vibrational stretching modes of the tetrahedra. The mid- to weak-strength peaks in the 700–900 cm–1 region (Group IV) belong to the deformation modes of the tetrahedra." (Freeman et al., 2008, see please their Figure 3, where Groups IV and V are given in the range of IR active modes).

"Several studies have been undertaken to describe the infrared spectra of albite [127–130], microcline and sanidine" (see Jovanovski & Makreski, 2016, and literature therein, Moenke, 1962, 1966, Couty & Velde, 1986, Johnson & Rossman, 2003). "The infrared vibrational spectra of the alkali feldspars (albite, microcline and sanidine) [see the Fig. 17a–c in Jovanovski & Makreski, 2016] were, to some extent, similar. Their main characteristic is the existence of bands in four regions. The highest-frequency region, adopting the bands in the 1200–850 cm^{-1} region followed by the bands between 800 and 700 cm^{-1}, could be used to discriminate between these minerals. On the other hand, the bands in the third region (700–350 cm^{-1}) indicate that the samples are crystalline since they are not present in the corresponding glasses [Jovanovski & Makreski, mentioning Couty & Velde, 1986]. Spectral variations in terms of the number of bands, as well as

variations in band intensities, were observed at the lowest wavenumbers (far-IR spectra, below 350 cm^{-1})" (Jovanovski & Makreski, 2016). "An increase of the Al/Si disorder degree in alkali feldspars is manifested by a decrease of IR band intensities, frequency band shifting and an increase of their widths" (Jovanovski & Makreski, 2016, mentioning Salje et al., 1989, Zhang et al., 1996).
Returning to Raman spectroscopy, the Al-Si ordering in albite has been studied by means of "A combined single-crystal X-ray diffraction and Raman spectroscopy" (Tribaudino et al., 2018). "The Raman spectra show a significant broadening with disorder, as well as some slight peak shift. Different peaks show different response to Al-Si disorder". "Three strong peaks, at 290 cm^{-1} (ν_c), 478 cm^{-1} (ν_b) and 507 cm^{-1} (ν_a) in ordered albite, were examined … . ν_c and ν_b show a red-shift with broadening and Al-Si disorder; ν_a blue-shifts with disorder and shows only a minor broadening. The broadening and shifts in Raman spectra are caused by structural deformation associated with Al-Si disorder. The ν_a peak at 507 cm^{-1} is the least affected by Al-Si disorder, and is suitable to assess compositional changes in plagioclase" (Tribaudino et al., 2018).
In Aliatis et al., 2015, a "comparison between ab initio calculated and measured Raman spectrum of triclinic albite" was proposed. "To give a rough picture of the agreement between ab initio calculations and experimental results, … the simulated spectrum for a polycrystalline isotropic sample, at excitation wavelength of 632.8 nm and temperature of 300 K, and assuming an overall *Lorentzian broadening* of 8 cm^{-1}, is compared with an experimental spectrum obtained by averaging the spectra …" (Aliatis et al., 2015). Here in the following, we assume the Raman spectra of Albite decomposed by means of q-Gaussian functions.

q-Gaussian function and its asymmetric q-BWF form
The fitting of Raman spectra with q-Gaussian line shapes has been proposed for the first time [in 2023] by A. C. Sparavigna. The q-Gaussian line shape is a function based on the Tsallis q-form of the exponential function (Tsallis, 1988). This exponential form is characterized by a q-parameter. When q is equal to 2, we have the Lorentzian function. If q is close to 1, we have a Gaussian function. For values of q between 1 and 2, we have a bell-shaped symmetric function with power-law wings ranging from Gaussian to Lorentzian tails.
The q-Gaussian is given as $f(x) = Ce_q(-\gamma x^2)$, where $e_q(.)$ is the q-exponential function and C a scale constant (Hanel et al., 2009). The q-exponential has expression: $e_q(u) = [1 + (1-q)u]^{1/(1-q)}$. For spectroscopy, we write the q-Gaussian function with the center of the band at x_o:

$$q\text{-}Gaussian = Cexp_q(-\gamma(x-x_o)^2) = C\,[1 + (q-1)\gamma(x-x_o)^2]^{1/(1-q)}.$$

We can apply q-Gaussian functions by means of Fityk software. In Fityk, a q-Gaussian function can be defined in the following manner:

```
define Qgau(height, center, hwhm, q=1.5) = height*(1+(q-1)*((x-center)/hwhm)^2)^(1/(1-q))
```

where q=1.5 is the initial guessed value of the q-parameter. Parameter hwhm is the half width at half maximum of the line, in the case of a Lorentzian function. In fact, when q=2, the q-Gaussian turns into a Lorentzian function, that we can find defined in Fityk as:

```
Lorentzian(height, center, hwhm) = height/(1+((x-center)/hwhm)^2)
```

When q is close to 1, the q-Gaussian becomes a Gaussian function.

In Fityk, to define a function, use please Session > New Script > Blank Fityk Script

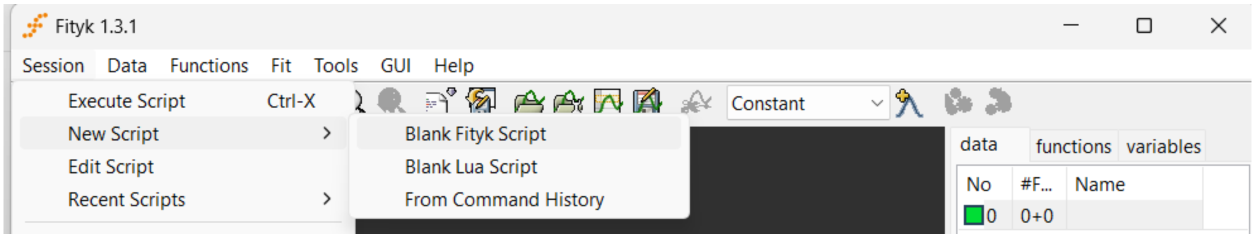

In the Blank Fityk Script paste the "define" of the function, for instance the Qgau given above.

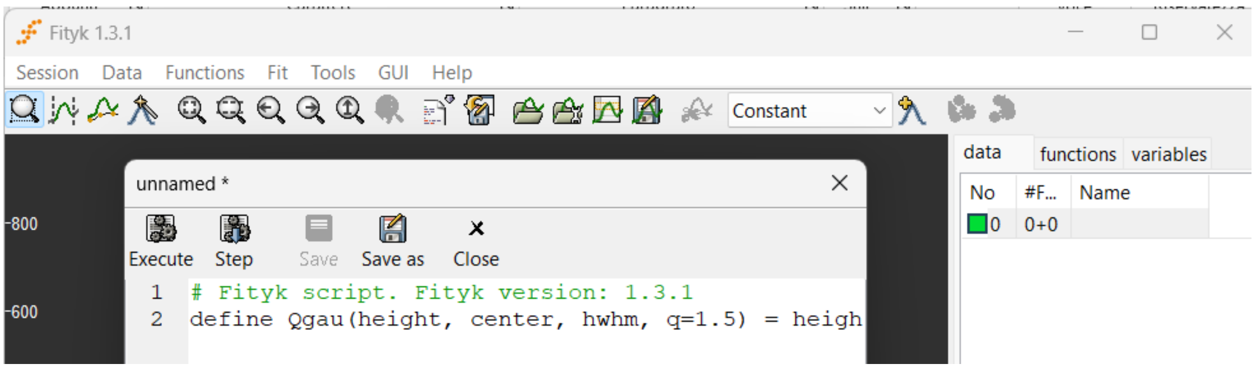

Then, save the Script, and execute it. Using Functions > Definition Manager, in the list of the functions, it will be the q-Gaussian function too.

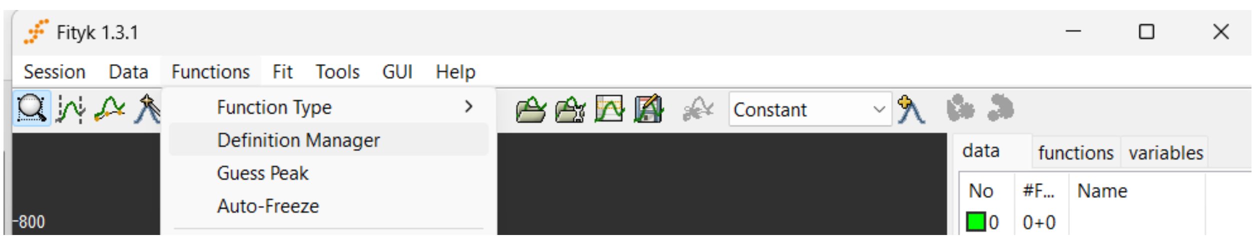

As shown on many occasions, the q-Gaussians are suitable for fitting Raman spectra (by examples proposed in SSRN to the SERS cases, for instance). For applying the q-Gaussians to asymmetric bands, we can define also an asymmetric function, turning the Breit-Wigner-Fano (BWF) function into a q-BWF function (Sparavigna, 2023). Let us write the BWF as follow:

$$\mathrm{BWF}(x) = C\,\frac{\left[1-\xi\gamma^{1/2}(x-x_o)\right]^2}{\left[1+\gamma(x-x_o)^2\right]}$$

When asymmetry parameter ξ is zero, BWF becomes a symmetric Lorentzian function. Note that the center of the line does not correspond to the position of the peak of the function. As in Sparavigna, 2023, we can define the q-BWF function in the following manner:

$$\text{q-BWF} = C\left[1-\xi\gamma^{1/2}(q-1)^{1/2}(x-x_o)\right]^2\left[1+(q-1)\gamma(x-x_o)^2\right]^{1/(1-q)}$$

In fact, the Lorentzian function is substituted by a q-Gaussian function.
In Fityk, the q-Breit-Wigner-Fano (q-BWF) can be defined as:

Qbreit(height, center, hwhm, q=1.5, xi=0.1) = (1-xi*(q-1)*(x-center)/hwhm)^2 * height*(1+(q-1)^0.5 *((x-center)/hwhm)^2)^(1/(1-q))

And the BWF can be defined as:

Breit(height, center, hwhm, xi=0.1) = (1-xi*(x-center)/hwhm)^2 * height/(1+((x-center)/hwhm)^2)

Using +xi instead of −xi does not change the fitting results in Fityk.

In the following work, we provide the Raman and ATR-IR spectral deconvolutions for Albite in the form of screenshots of Fityk software, where the green dots are data from RRUFF, red curves the q-Gaussian components (or q-BWF components), yellow curve the sum of components. In the lower part of the screenshot, the misfit is given (difference between data and yellow curve). Supplementary material is providing folders containing .txt RRUFF data and the Fityk files .fit and .peaks, Mendeley Data, V1, https://data.mendeley.com/datasets/74b2fw4fw4/1 .

Raman fingerprints

Albite R040068 (Raman, depolarized)

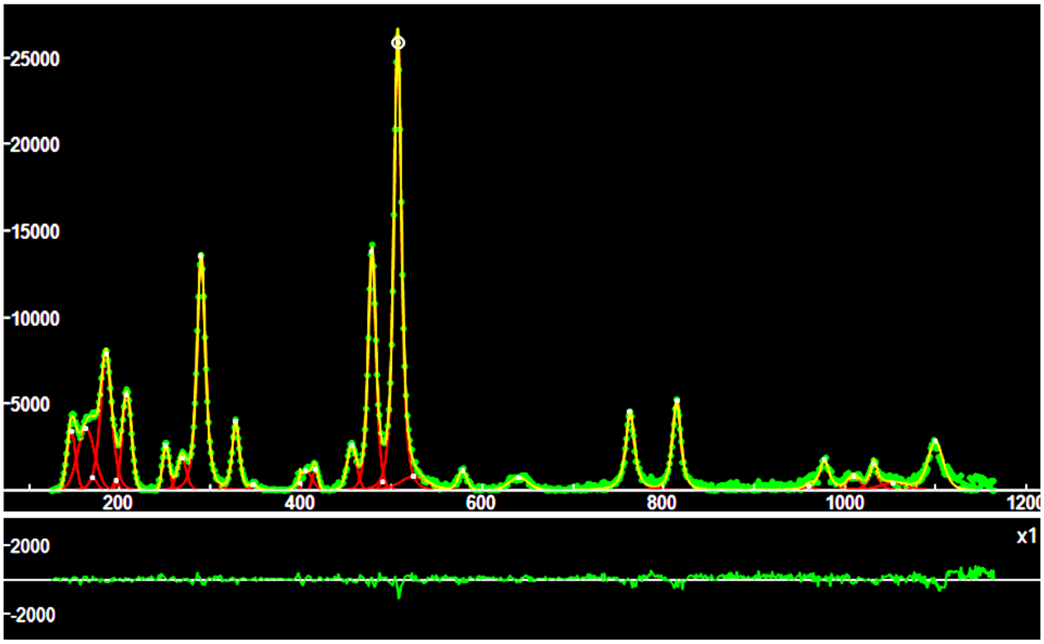

# PeakType		Center				Height (H>1000)	Center	HWHM	q-parameter
%_8	Qgau	146.62	x	x	x	3412.67	146.62	6.74194	1.00001
%_20	Qgau	162.896	x	x	x	3596.74	162.896	13.3251	1.02111
%_4	Qgau	184.936	x	x	x	7947.85	184.936	8.2116	1.36103
%_11	Qgau	207.929	x	x	x	5586.41	207.929	7.12756	1.01458
%_12	Qgau	251.02	x	x	x	2633.06	251.02	5.17182	1.00143
%_15	Qgau	268.493	x	x	x	1879.37	268.493	6.90934	1.23025
%_3	Qgau	289.873	x	x	x	13688.8	289.873	5.91685	1.54832
%_13	Qgau	296	x	x	x	1750.64	977.296	6.31406	2.04987
%_7	Qgau	328.062	x	x	x	4002.59	328.062	4.89543	1.53632
%_27	Qgau	405.143	x	x	x	1141.96	405.143	10.0224	0.999881
%_29	Qgau	415.627	x	x	x	1225.85	415.627	4.35547	1.0015
%_10	Qgau	455.969	x	x	x	2578.97	455.969	7.07977	1.16447
%_2	Qgau478.365		x	x	x	13856.8	478.365	5.59592	1.40925
%_1	Qgau506.596		x	x	x	26239.4	506.596	5.26768	1.58821
%_18	Qgau578.109		x	x	x	1155.93	578.109	6.62098	1.21043
%_6	Qgau763.099		x	x	x	4569.24	763.099	5.86456	1.81766
%_5	Qgau814.354		x	x	x	5223.19	814.354	5.72984	1.66114
%_14	Qgau1031.78		x	x	x	1584.73	1031.78	4.99419	1.91284
%_9	Qgau1099.73		x	x	x	2813.15	1099.73	11.3849	1.35074

Albite R040129 (Raman, depolarized)

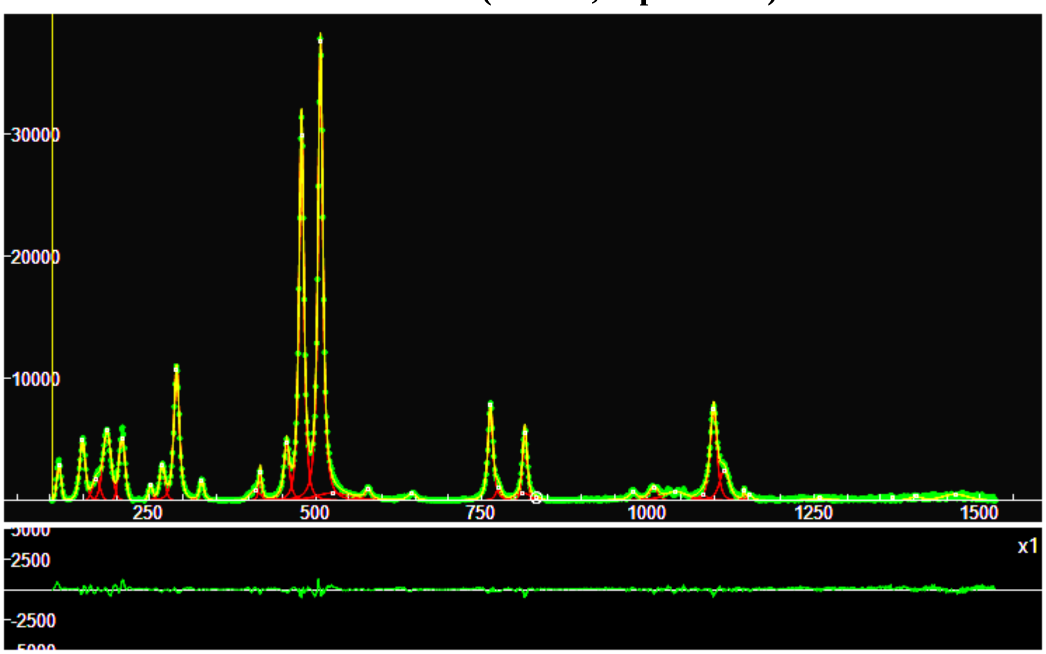

# PeakType		Center				Height (H>900)	Center	HWHM	q-parameters...
%_11	Qgau	113.33	x	x	x	2904.74	113.33	4.59998	1.00035
%_9	Qgau	148.693	x	x	x	5110.4	148.693	5.32436	1.49661
%_17	Qgau	169.371	x	x	x	1763.81	169.371	8.01116	1.00162

%_8	Qgau	185.675	x	x	x	5697.39	185.675	8.28261	1.18188
%_6	Qgau	208.103	x	x	x	5206.96	208.103	6.49248	1.00398
%_19	Qgau	251.265	x	x	x	1211.52	251.265	4.50638	1.00699
%_12	Qgau	268.769	x	x	x	2915.45	268.769	5.29467	1.33297
%_3	Qgau	290.378	x	x	x	11136.7	290.378	4.98692	1.62712
%_16	Qgau	328.181	x	x	x	1741.86	328.181	3.81368	1.64972
%_14	Qgau	416.223	x	x	x	2297.76	416.223	2.28202	1.74623
%_10	Qgau	456.06	x	x	x	4729.15	456.06	4.56657	1.85425
%_2	Qgau	478.431	x	x	x	31380	478.431	4.40716	1.66113
%_1	Qgau	506.988	x	x	x	37606.1	506.988	4.35223	1.79922
%_20	Qgau	578.827	x	x	x	967.132	578.827	5.25452	1.94126
%_23	Qgau	775.18	x	x	x	982.818	775.18	5.26577	1.67754
%_4	Qgau	762.91	x	x	x	7879.3	762.91	4.53413	1.7164
%_7	Qgau	814.726	x	x	x	5611.95	814.726	4.25355	1.39673
%_18	Qgau	1008.68	x	x	x	1031.76	1008.68	8.72407	1.22323
%_5	Qgau	1098.85	x	x	x	7600.55	1098.85	6.27887	1.53802
%_15	Qgau	1115.05	x	x	x	2470.56	1115.05	9.46927	1.51387

Albite R050253 (Raman, depolarized)

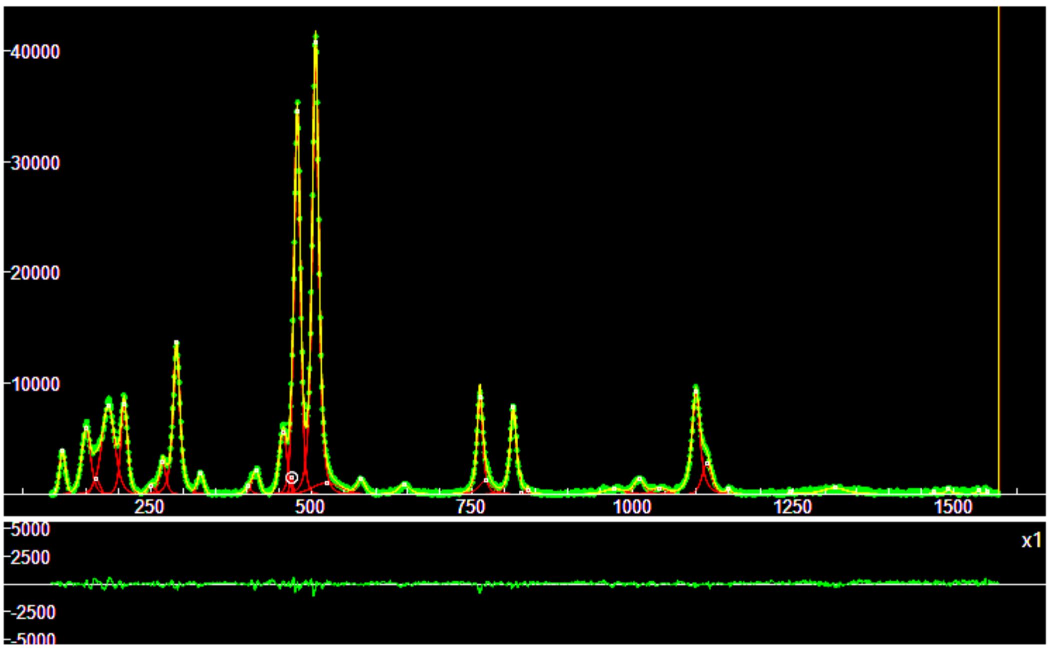

#	PeakType	Center				Height(H>1500)	Center	HWHM	q-parameters...
%_11	Qgau	112.318	x	x	x	3908.91	112.318	6.41437	1.001
%_9	Qgau	149.025	x	x	x	6004.71	149.025	8.9046	1.38976
%_7	Qgau	183.471	x	x	x	7990.5	183.471	13.1469	1.32982
%_6	Qgau	208.225	x	x	x	8119	208.225	6.74264	1.37753
%_12	Qgau	268.295	x	x	x	2979.18	268.295	6.31219	1.50922
%_3	Qgau	289.895	x	x	x	13804.5	289.895	6.49452	1.62584

%_15	Qgau	327.322	x	x	x	1887.23	327.322	6.96588	1.00196
%_13	Qgau	413.584	x	x	x	2155.05	413.584	8.11489	1.0425
%_10	Qgau	455.726	x	x	x	5654.47	455.726	8.45983	1.08988
%_25	Qgau	468.64	x	x	x	1674.91	468.64	3.33664	1.00323
%_2	Qgau	477.872	x	x	x	34653	477.872	6.3741	1.3654
%_1	Qgau	506.373	x	x	x	40900.5	506.373	6.31799	1.57078
%_5	Qgau	762.488	x	x	x	9035.99	762.488	5.23792	1.6991
%_8	Qgau	814.396	x	x	x	7966.51	814.396	5.98807	1.66605
%_4	Qgau	1098.96	x	x	x	9324.1	1098.96	7.57244	1.75637
%_14	Qgau	1115.71	x	x	x	2749.43	1115.71	9.93138	1.31582

Albite R050402 (Raman, depolarized)

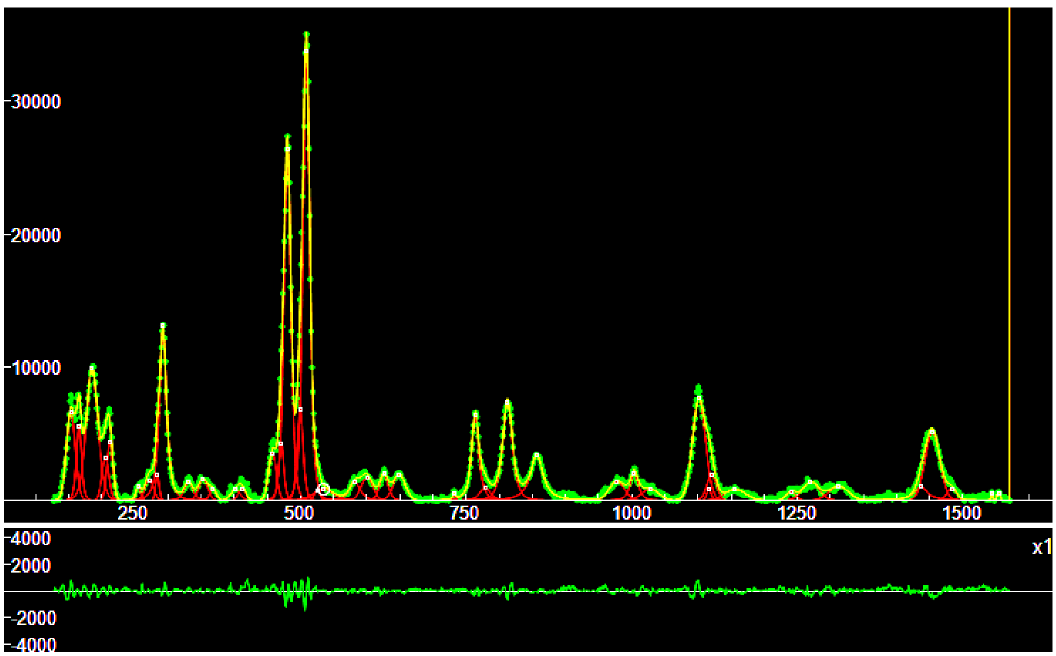

# PeakType		Center				Height(H>1100)	Center ..	HWHM ..	q-parameters
%_9	Qgau	153.559	x	x	x	6761.05	153.559	9.20214	1.05608
%_25	Qgau	165.804	x	x	x	5641.51	165.804	5.03952	1.33914
%_4	Qgau	185.524	x	x	x	9970.21	185.524	11.8804	1.19092
%_36	Qgau	205.655	x	x	x	3241.9	205.655	7.56039	1.00001
%_23	Qgau	212.38	x	x	x	4395.17	212.38	6.39902	1.00144
%_19	Qgau	271.774	x	x	x	1561.67	271.774	9.22548	1.00126
%_33	Qgau	284.011	x	x	x	1935.26	284.011	3.941	1.00038
%_3	Qgau	292.59	x	x	x	13272.3	292.59	6.45048	1.65957
%_38	Qgau	331.172	x	x	x	1384.97	331.172	8.38212	1.51187
%_14	Qgau	353.156	x	x	x	1588.58	353.156	9.87973	1.00392
%_11	Qgau	457.818	x	x	x	3563.76	457.818	8.20431	1.00307
%_22	Qgau	471.16	x	x	x	4413.12	471.16	4.96767	1.35119
%_2	Qgau	480.351	x	x	x	26681.3	480.351	6.77458	1.32781
%_46	Qgau	499.77	x	x	x	6907.48	499.77	5.89935	1.30178

%_1	Qgau	509.014	x	x	x	33786.4	509.014	6.48298	1.40985
%_17	Qgau	582.047	x	x	x	1391.18	582.047	10.6739	1.5533
%_41	Qgau	600.403	x	x	x	1748.64	600.403	12.5737	1.00366
%_13	Qgau	626.018	x	x	x	2029.84	626.018	8.36747	1.29448
%_28	Qgau	649.225	x	x	x	1969.65	649.225	12.9742	1.00427
%_7	Qgau	763.923	x	x	x	6412.12	763.923	6.72417	1.70067
%_6	Qgau	812.588	x	x	x	7425.99	812.588	9.37716	1.53138
%_10	Qgau	856.731	x	x	x	3412.58	856.731	11.6856	1.85346
%_18	Qgau	977.707	x	x	x	1433.29	977.707	16.2823	1.00935
%_12	Qgau	1003.8	x	x	x	2066.78	1003.8	7.6447	1.62781
%_5	Qgau	1101.62	x	x	x	7702.15	1101.62	13.3225	1.08584
%_15	Qgau	1270.22	x	x	x	1412.74	1270.22	17.2821	1.07997
%_24	Qgau	1120.74	x	x	x	1916.84	1120.74	10.5942	1.00308
%_8	Qgau	1453.9	x	x	x	5093.74	1453.9	15.7564	1.01447

Albite R060054 (Raman, unoriented, 532)

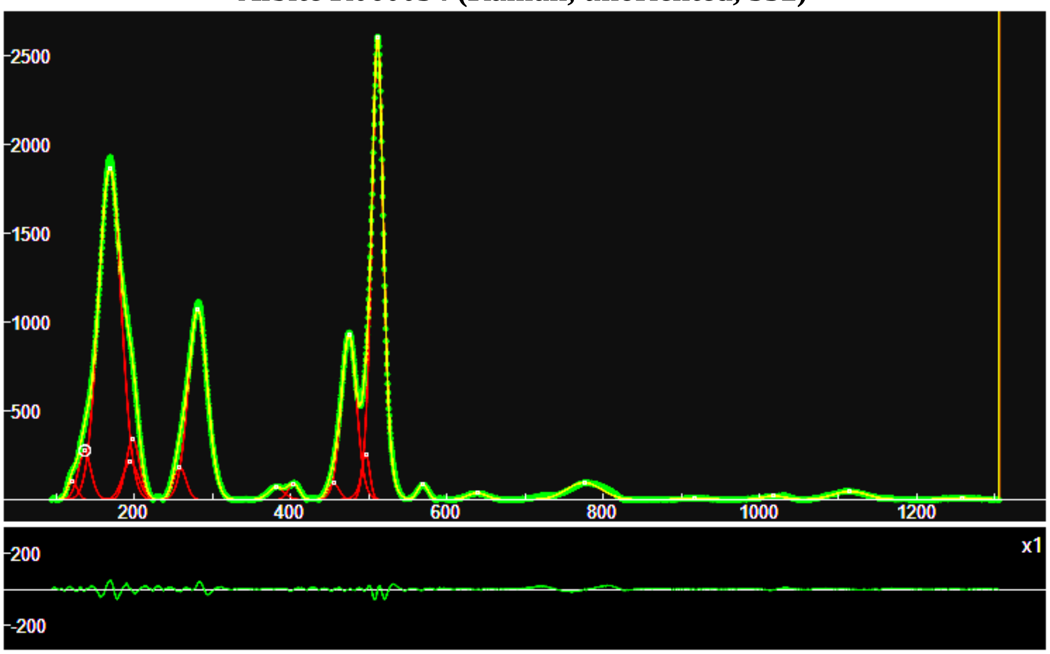

# PeakType		Center				Height(H>50)	Center	HWHM	q-parameters...
%_18	Qgau	121.043	x	x	x	104.183	121.043	8.80457	1.00389
%_21	Qgau	136.602	x	x	x	274.466	136.602	11.2213	1.15549
%_2	Qgau	168.707	x	x	x	1867.27	168.707	20.2536	1.00641
%_19	Qgau	195.199	x	x	x	213.768	195.199	14.398	0.999832
%_6	Qgau	198.111	x	x	x	342.901	198.111	12.0568	1.00367
%_10	Qgau	258.286	x	x	x	184.496	258.286	11.2147	1.00143
%_3	Qgau	281.363	x	x	x	1073.23	281.363	16.8139	1.05767
%_13	Qgau	381.528	x	x	x	72.8141	381.528	13.5232	1.15533
%_7	Qgau	403.774	x	x	x	89.0932	403.774	10.2657	1.0006

%_20	Qgau	454.679	x	x	x	93.2535	454.679	10.3275	1.00047
%_4	Qgau	474.495	x	x	x	930.775	474.495	13.4364	1.09498
%_17	Qgau	495.989	x	x	x	260.068	495.989	7.1236	1.00534
%_1	Qgau	511.074	x	x	x	2605.68	511.074	9.99489	1.27121
%_9	Qgau	568.834	x	x	x	86.7513	568.834	9.29742	1.00656
%_5	Qgau	775.27	x	x	x	96.8436	775.27	31.6579	0.998828

Albite R060054 (Raman, unoriented, 785)

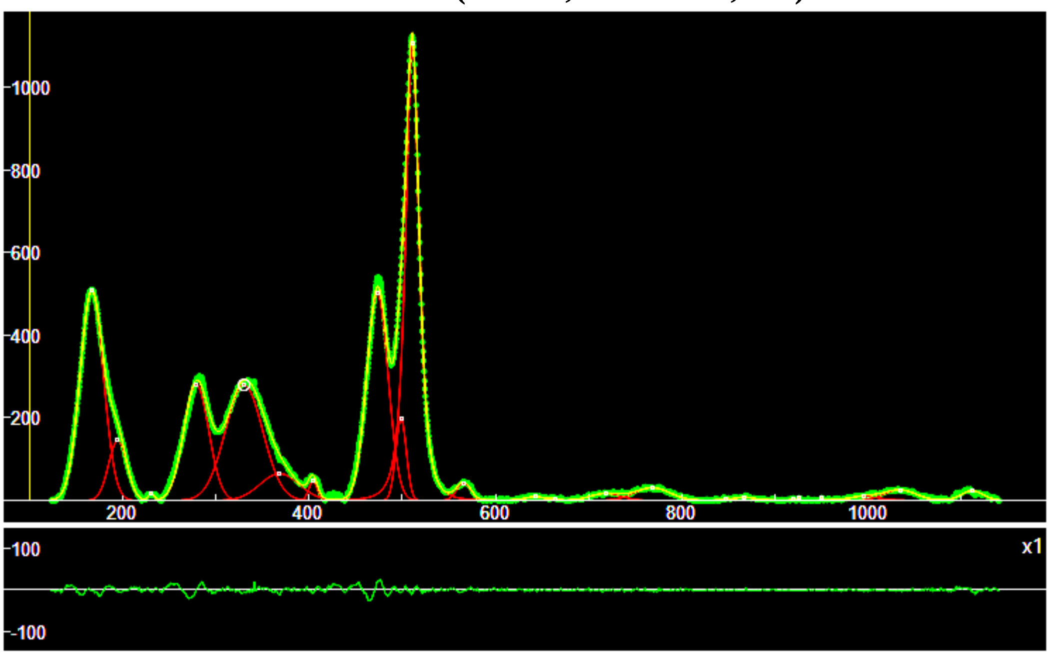

#	PeakType	Center				Height(H>20)	. Center..	HWHM	q-parameters...
%_2	Qgau	166.311	x	x	x	508.661	166.311	17.6302	1.00001
%_16	Qgau	194.265	x	x	x	145.563	194.265	13.8006	1.00213
%_4	Qgau	278.618	x	x	x	281.135	278.618	18.9022	1.00012
%_5	Qgau	329.926	x	x	x	279.867	329.926	28.304	0.998932
%_17	Qgau	368.069	x	x	x	65.2843	368.069	29.5839	0.999429
%_11	Qgau	403.984	x	x	x	46.7146	403.984	6.49969	0.999949
%_3	Qgau	473.15	x	x	x	502.354	473.15	16.2043	1.00109
%_8	Qgau	498.522	x	x	x	199.194	498.522	8.01197	1.00065
%_1	Qgau	510.707	x	x	x	1110.15	510.707	9.26977	1.54914
%_6	Qgau	565.813	x	x	x	40.9986	565.813	10.9433	1.00009
%_7	Qgau	768.321	x	x	x	31.0855	768.321	26.7993	1.00015
%_9	Qgau	1034.32	x	x	x	25.2857	1034.32	24.7228	0.999301
%_10	Qgau	1111.73	x	x	x	23.4968	1111.73	17.0883	1.00103

Albite R070268 (Raman, unoriented, 532)

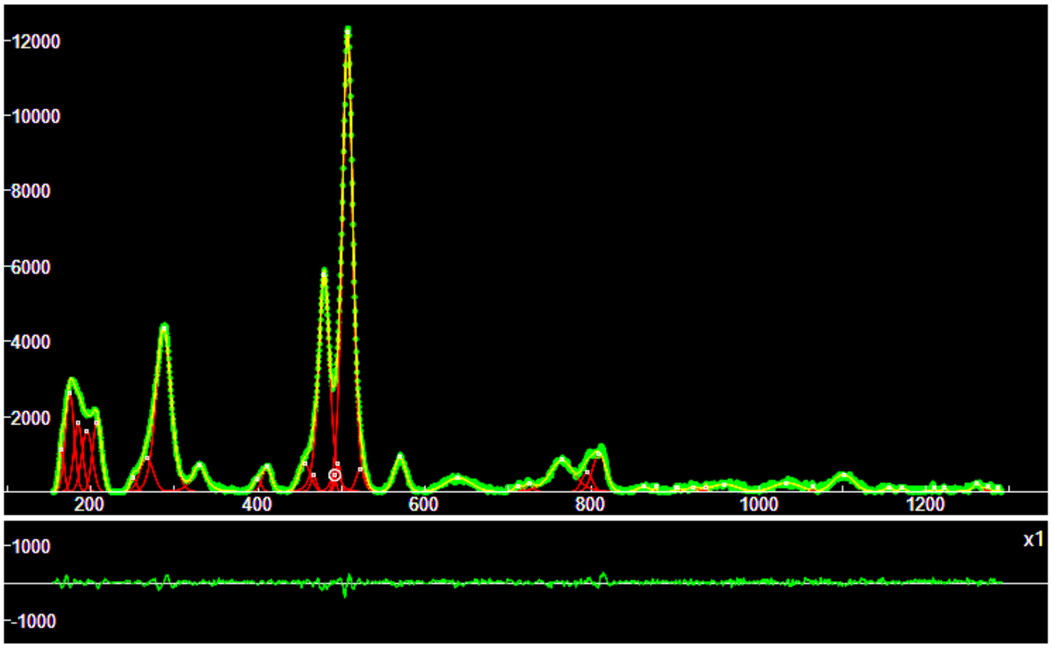

# PeakType		Center				Height(H>400)	Center	HWHM	q-parameters...
%_40	Qgau	164.733	x	x	x	1144.04	164.733	4.38568	1.00344
%_34	Qgau	174.396	x	x	x	2627.58	174.396	7.37908	1.00581
%_39	Qgau	184.427	x	x	x	1818.49	184.427	7.25916	1.12116
%_35	Qgau	194.985	x	x	x	1629.13	194.985	8.89006	1.00294
%_8	Qgau	207.08	x	x	x	1873.76	207.08	7.66917	1.00578
%_14	Qgau	266.404	x	x	x	910.278	266.404	11.4686	1.00194
%_3	Qgau	286.803	x	x	x	4356.62	286.803	12.0863	1.16257
%_10	Qgau	329.325	x	x	x	726.711	329.325	10.1722	1.59652
%_9	Qgau	410.599	x	x	x	664.722	410.599	7.50284	1.11412
%_11	Qgau	455.93	x	x	x	736.328	455.93	10.0741	1.00516
%_16	Qgau	466.734	x	x	x	445	466.734	4.2312	1.46544
%_2	Qgau	479.261	x	x	x	5824.67	479.261	8.49715	1.37441
%_37	Qgau	491.413	x	x	x	451.013	491.413	2.90459	1.27295
%_41	Qgau	496.075	x	x	x	754.882	496.075	4.22849	1.00015
%_1	Qgau	507.271	x	x	x	12222	507.271	8.35653	1.23601
%_42	Qgau	523.097	x	x	x	616.893	523.097	7.82935	1.04812
%_6	Qgau	569.917	x	x	x	921.409	569.917	10.0344	1.00141
%_7	Qgau	764.305	x	x	x	843.987	764.305	19.1267	1.3429
%_24	Qgau	794.158	x	x	x	514.304	794.158	9.15787	1.00008
%_5	Qgau	808.805	x	x	x	1000.38	808.805	11.368	1.00295
%_12	Qgau	1101.47	x	x	x	460.888	1101.47	17.7053	1.0004

Albite R070268 (Raman, unoriented, 785)

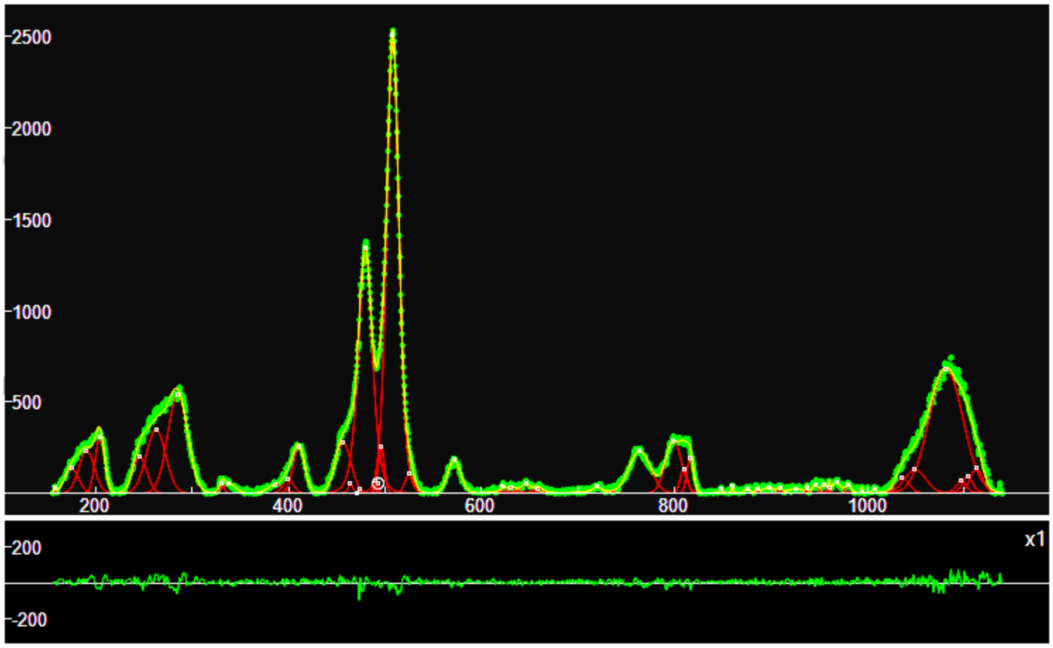

# PeakType		Center				Height(H>70)	Area	HWHM	q-parameters...
%_13	Qgau	175.059	x	x	x	136.331	175.059	10.1006	1.00013
%_32	Qgau	190.678	x	x	x	235.835	190.678	11.2591	0.999982
%_6	Qgau	204.51	x	x	x	307.232	204.51	6.97042	1.0003
%_33	Qgau	245.753	x	x	x	199.801	245.753	10.2928	1.00003
%_11	Qgau	262.434	x	x	x	349.687	262.434	14.221	0.999794
%_4	Qgau	285.098	x	x	x	542.537	285.098	14.5899	1.00042
%_46	Qgau	399.653	x	x	x	75.7476	399.653	7.93613	1.00135
%_7	Qgau	410.536	x	x	x	255.196	410.536	8.55294	1.00126
%_8	Qgau	456.449	x	x	x	277.446	456.449	11.4413	1.0002
%_51	Qgau	471.349	x	x	x	75.8969	471.349	0.0846984	1.45596
%_2	Qgau	479.449	x	x	x	1340.82	479.449	9.60717	1.31323
%_20	Qgau	495.944	x	x	x	258.463	495.944	4.43444	1.0004
%_1	Qgau	507.882	x	x	x	2520.66	507.882	8.4938	1.2081
%_47	Qgau	525.126	x	x	x	105.294	525.126	6.52119	0.999917
%_10	Qgau	571.447	x	x	x	183.491	571.447	9.1916	1.08376
%_9	Qgau	763.589	x	x	x	230.81	763.589	15.6172	1.01624
%_5	Qgau	798.648	x	x	x	287.464	798.648	11.5878	1.01384
%_35	Qgau	809.235	x	x	x	133.74	809.235	5.14179	1.00005
%_12	Qgau	815.972	x	x	x	196.577	815.972	4.94703	1.00027
%_41	Qgau	1035.64	x	x	x	82.3841	1035.64	10.2454	1.00017
%_17	Qgau	1048.93	x	x	x	128.334	1048.93	15.9253	0.999734
%_3	Qgau	1080.9	x	x	x	683.049	1080.9	24.6113	0.999735
%_49	Qgau	1096.76	x	x	x	70.5165	1096.76	6.91652	1.33916
%_45	Qgau	1103.33	x	x	x	95.3051	1103.33	6.9451	1.2872
%_36	Qgau	1112.48	x	x	x	137.315	1112.48	9.16133	1.00033

Albite R100169 (Raman, unoriented, 532)

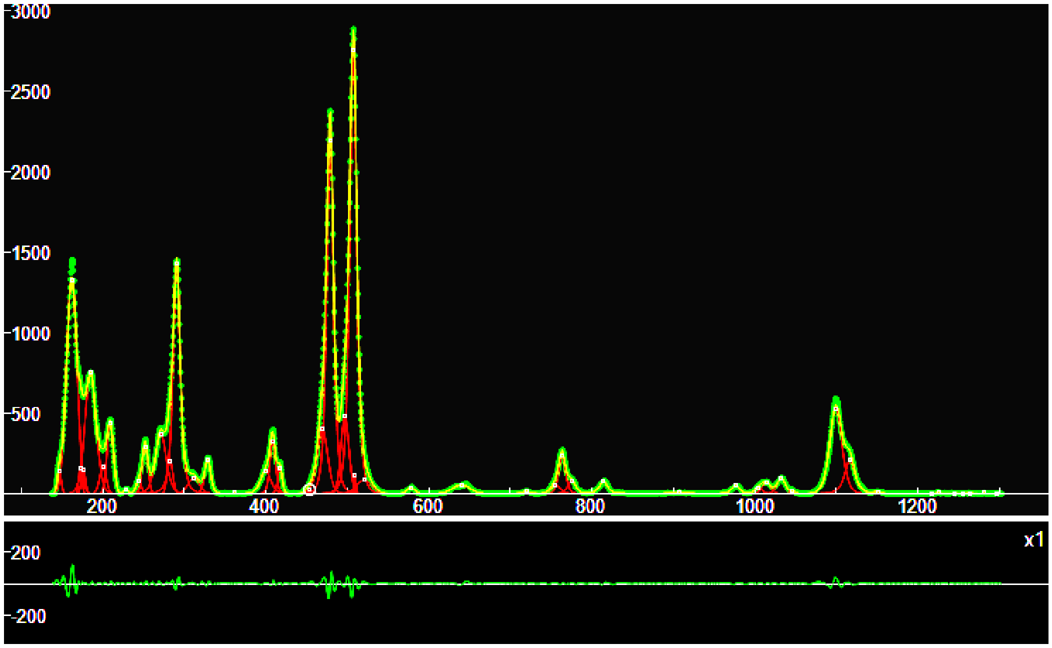

# PeakType		Center				Height(H>50)	Center	HWHM	q-parameters...
%_36	Qgau	146.969	x	x	x	141.422	146.969	3.23122	1.00225
%_3	Qgau	161.922	x	x	x	1337.14	161.922	8.978	1.00008
%_30	Qgau	172.444	x	x	x	171.597	172.444	2.65977	1.00014
%_37	Qgau	176.408	x	x	x	153.244	176.408	3.5397	1.00296
%_5	Qgau	184.968	x	x	x	750.782	184.968	9.28693	1.12671
%_28	Qgau	200.117	x	x	x	166.603	200.117	5.7155	1.00295
%_8	Qgau	209.063	x	x	x	438.347	209.063	5.61029	1.00216
%_34	Qgau	244.197	x	x	x	75.4112	244.197	4.90147	0.999982
%_13	Qgau	251.994	x	x	x	299.428	251.994	4.65747	1.0974
%_9	Qgau	271.163	x	x	x	372.938	271.163	8.85026	1.2761
%_26	Qgau	282.625	x	x	x	207.369	282.625	4.79606	1.0032
%_4	Qgau	290.694	x	x	x	1431.62	290.694	5.34578	1.53444
%_20	Qgau	311.692	x	x	x	97.0603	311.692	10.3013	1.00128
%_11	Qgau	328.671	x	x	x	214.726	328.671	4.79955	1.29993
%_22	Qgau	399.861	x	x	x	140.198	399.861	8.50917	1.30507
%_7	Qgau	408.406	x	x	x	327.368	408.406	4.63764	1.2306
%_21	Qgau	417.31	x	x	x	157.208	417.31	3.80385	1.1507
%_14	Qgau	469.62	x	x	x	402.302	469.62	8.64624	1.19742
%_2	Qgau	479.021	x	x	x	2219.78	479.021	5.43029	1.43202
%_12	Qgau	497.189	x	x	x	478.496	497.189	6.97578	1.0011
%_1	Qgau	507.32	x	x	x	2755.54	507.32	5.55286	1.44188
%_48	Qgau	509.449	x	x	x	120.616	509.449	1.69017	1.00158
%_27	Qgau	520.885	x	x	x	85.2292	520.885	13.4498	1.00293
%_19	Qgau	639.867	x	x	x	55.5649	639.867	15.5926	0.999598

%_29	Qgau	755.764	x	x	x	52.7508	755.764	8.76315	1.10558
%_10	Qgau	763.595	x	x	x	235.4	763.595	5.47324	1.32191
%_23	Qgau	775.305	x	x	x	79.24	775.305	6.5211	1.35637
%_17	Qgau	814.323	x	x	x	80.8427	814.323	5.92307	1.80414
%_18	Qgau	1014.04	x	x	x	66.8939	1014.04	8.00268	1.00076
%_16	Qgau	1032.3	x	x	x	94.2769	1032.3	7.60092	1.11332
%_6	Qgau	1099.39	x	x	x	529.093	1099.39	10.0696	1.23981
%_15	Qgau	1116.57	x	x	x	208.594	1116.57	7.99277	1.5707

Albite R100169 (Raman, unoriented, 780)

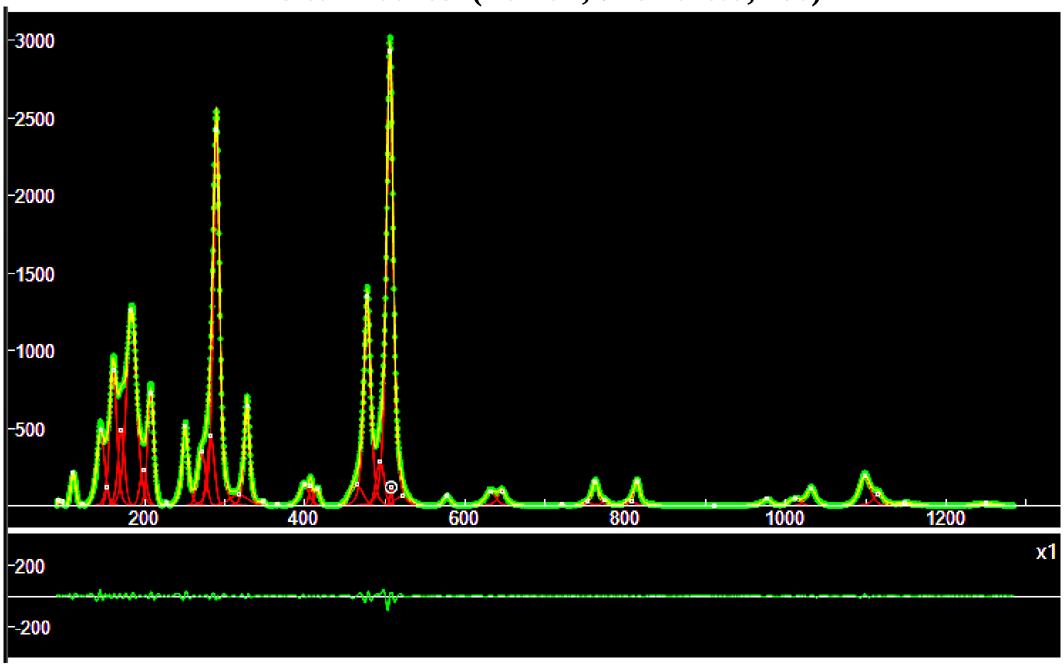

# PeakType		Center				Height(H>100)	Center	HWHM	q-parameters...
%_14	Qgau	110.919	x	x	x	220.372	110.919	4.23309	1.00392
%_8	Qgau	145.125	x	x	x	489.988	145.125	6.46384	1.28119
%_33	Qgau	152.953	x	x	x	119.819	152.953	2.93226	1.00631
%_7	Qgau	160.74	x	x	x	887.448	160.74	5.66153	1.29318
%_39	Qgau	170.672	x	x	x	486.814	170.672	5.61726	1.14783
%_4	Qgau	183.642	x	x	x	1269.54	183.642	8.58345	1.18349
%_42	Qgau	198.425	x	x	x	233.867	198.425	5.86381	1.08066
%_10	Qgau	207.649	x	x	x	725.183	207.649	5.45389	1.06139
%_6	Qgau	250.526	x	x	x	519.322	250.526	4.6682	1.5335
%_9	Qgau	271.163	x	x	x	346.238	271.163	7.18408	1.00333
%_45	Qgau	282.552	x	x	x	450.166	282.552	6.2323	1.00012
%_2	Qgau	289.667	x	x	x	2435.51	289.667	4.80969	1.50654
%_5	Qgau	327.675	x	x	x	659.807	327.675	4.02028	1.48994
%_38	Qgau	399.005	x	x	x	138.309	399.005	7.4537	1.32542
%_13	Qgau	407.386	x	x	x	133.978	407.386	3.37493	1.08664
%_40	Qgau	415.584	x	x	x	106.353	415.584	4.27851	1.14238

%_41	Qgau	464.232	x	x	x	136.652	464.232	11.1676	1.0001
%_3	Qgau	477.754	x	x	x	1351.24	477.754	5.261	1.4862
%_44	Qgau	493.701	x	x	x	287.092	493.701	7.09769	1.00617
%_1	Qgau	505.986	x	x	x	2927.5	505.986	5.30683	1.49859
%_46	Qgau	507.732	x	x	x	121.737	507.732	1.61407	1.00636
%_16	Qgau	762.388	x	x	x	159.963	762.388	5.26182	1.41495
%_15	Qgau	814.108	x	x	x	160.663	814.108	4.34785	1.90608
%_17	Qgau	1031.5	x	x	x	113.388	1031.5	7.8877	1.28143
%_12	Qgau	1098.49	x	x	x	191.515	1098.49	8.88707	1.34478

Albite R230008 (Raman, depolarized, 532)

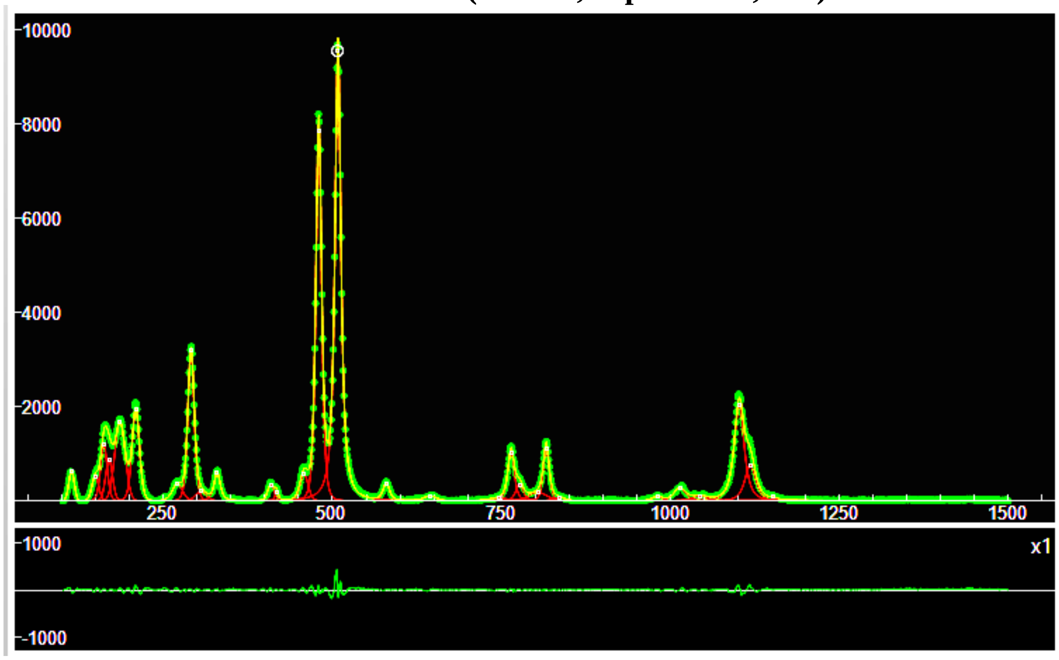

# PeakType		Center				Height	Center	HWHM	q-parameters...
%_11	Qgau	114.06	x	x	x	635.286	114.06	5.66013	1.00065
%_25	Qgau	149.231	x	x	x	520.139	149.231	7.10316	0.999975
%_9	Qgau	161.872	x	x	x	1189.79	161.872	6.69712	1.14548
%_33	Qgau	169.554	x	x	x	869.832	169.554	7.24103	1.04823
%_6	Qgau	185.709	x	x	x	1681.3	185.709	10.7804	0.99995
%_5	Qgau	209.06	x	x	x	1975.4	209.06	7.2655	1.22251
%_18	Qgau	270.671	x	x	x	359.254	270.671	10.3443	1.18701
%_3	Qgau	290.839	x	x	x	3196.18	290.839	6.25208	1.26479
%_28	Qgau	305.487	x	x	x	196.424	305.487	11.6089	1.00002
%_10	Qgau	329.458	x	x	x	608.918	329.458	5.65144	1.64233
%_14	Qgau	409.004	x	x	x	344.852	409.004	6.67505	1.05212
%_27	Qgau	417.455	x	x	x	176.547	417.455	3.69593	1.11986
%_12	Qgau	458.106	x	x	x	562.926	458.106	8.22742	1.12802
%_2	Qgau	479.683	x	x	x	7973.27	479.683	5.34862	1.45147
%_1	Qgau	508.157	x	x	x	9798.92	508.157	5.14264	1.84904

%_13	Qgau	579.56	x	x	x	369.253	579.56	6.32746	1.42028
%_22	Qgau	644.384	x	x	x	98.6916	644.384	13.4476	0.99989
%_32	Qgau	745.803	x	x	x	55.0011	745.803	20.5119	0.999698
%_8	Qgau	764.186	x	x	x	1054.56	764.186	6.13034	1.47272
%_19	Qgau	776.783	x	x	x	335.519	776.783	7.5937	1.36283
%_21	Qgau	803.722	x	x	x	175.717	803.722	19.5366	1.001
%_7	Qgau	816.226	x	x	x	1129.26	816.226	5.54696	1.4094
%_30	Qgau	835.354	x	x	x	69.8102	835.354	12.427	1.00511
%_24	Qgau	980.649	x	x	x	86.1926	980.649	10.9251	1.0421
%_17	Qgau	1013.66	x	x	x	267.008	1013.66	11.4996	1.36107
%_26	Qgau	1043.51	x	x	x	97.0693	1043.51	16.8899	1.37635
%_4	Qgau	1101.59	x	x	x	2035.12	1101.59	9.21574	1.64082
%_16	Qgau	1117.94	x	x	x	752.71	1117.94	10.2591	1.54762
%_29	Qgau	1152.13	x	x	x	80.6272	1152.13	2.43823	4.04598

Albite X050005 (Raman, unoriented, 785)

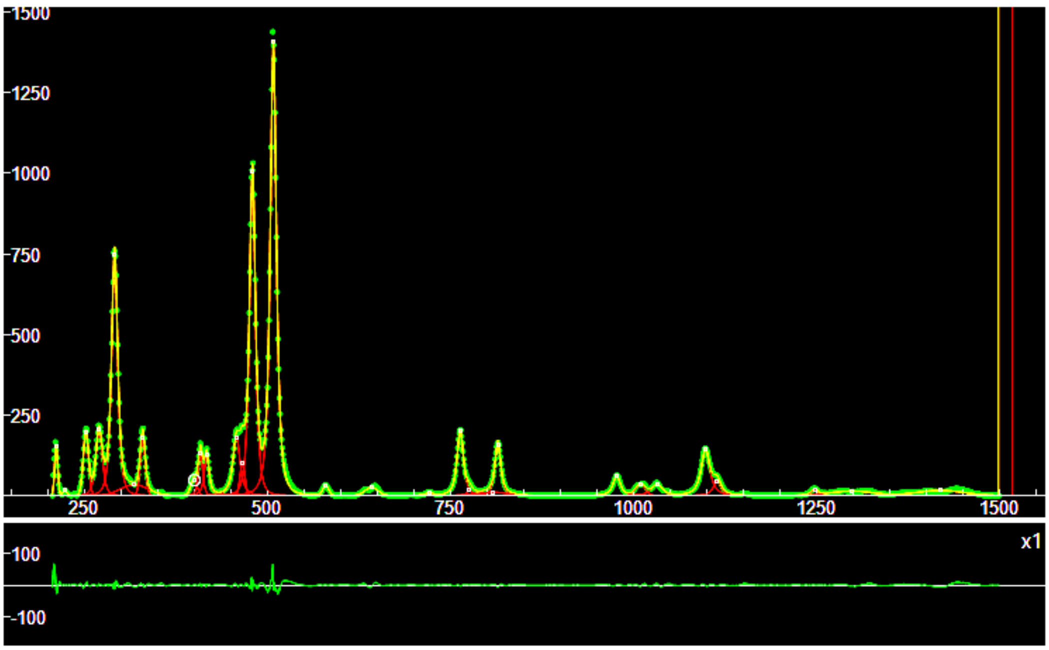

#	PeakType	Center				Height(H>20)	Center	HWHM	q-parameters...
%_9	Qgau	211.152	x	x	x	156.671	211.152	2.90649	0.999995
%_7	Qgau	251.677	x	x	x	197.137	251.677	4.95929	1.06226
%_4	Qgau	269.707	x	x	x	205.58	269.707	5.73103	1.48133
%_3	Qgau	290.974	x	x	x	756.548	290.974	5.17231	1.55659
%_33	Qgau	317.851	x	x	x	34.2212	317.851	26.6378	1.00319
%_5	Qgau	329.351	x	x	x	178.793	329.351	4.51465	1.14603
%_35	Qgau	399.312	x	x	x	46.8854	399.312	6.22805	1.00001
%_11	Qgau	408.292	x	x	x	134.38	408.292	3.82551	1.42285
%_15	Qgau	416.748	x	x	x	132.399	416.748	3.81022	1.76546
%_8	Qgau	457.548	x	x	x	180.966	457.548	5.96519	1.70609

%_34	Qgau	465.67	x	x	x	102.346	465.67	4.65259	1.00349
%_2	Qgau	479.352	x	x	x	1010.89	479.352	5.05724	1.57099
%_1	Qgau	507.857	x	x	x	1406.28	507.857	5.08692	1.67848
%_20	Qgau	579.417	x	x	x	31.7135	579.417	5.84585	1.00287
%_21	Qgau	642.181	x	x	x	25.6478	642.181	12.588	0.999976
%_6	Qgau	763.251	x	x	x	204.324	763.251	5.18121	1.75362
%_10	Qgau	814.661	x	x	x	161.185	814.661	4.81159	1.70111
%_14	Qgau	977.039	x	x	x	60.4621	977.039	6.4724	1.68406
%_19	Qgau	1009.46	x	x	x	33.2665	1009.46	9.59954	1.00089
%_16	Qgau	1032.14	x	x	x	34.6141	1032.14	9.31827	1.76577
%_12	Qgau	1098.44	x	x	x	143.442	1098.44	7.17764	1.79365
%_18	Qgau	1114.3	x	x	x	43.5453	1114.3	6.72017	1.76273

Albite X050006 (Raman, unoriented, 785)

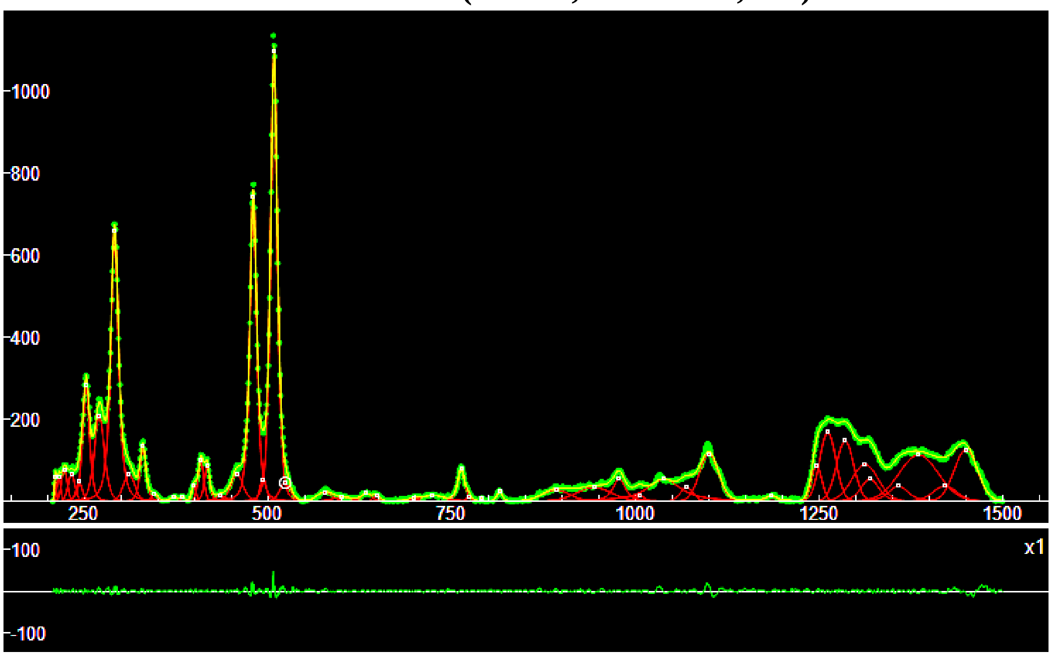

# PeakType		Center			Height(H>50)		Center	HWHM	q-parameters...
%_53	Qgau	210.139	x	x	x	63.5306	210.139	1.5812	1.00068
%_28	Qgau	214.779	x	x	x	59.0817	214.779	3.52302	1.001
%_49	Qgau	222.373	x	x	x	76.9474	222.373	5.43688	1.0013
%_48	Qgau	232.106	x	x	x	66.1868	232.106	6.57922	1.031
%_16	Qgau	242.63	x	x	x	46.7871	242.63	5.71979	1.24524
%_4	Qgau	252.009	x	x	x	280.678	252.009	5.91537	1.44512
%_13	Qgau	269.993	x	x	x	207.999	269.993	9.10227	1.30593
%_3	Qgau	290.868	x	x	x	661.119	290.868	6.38631	1.64162
%_14	Qgau	310.465	x	x	x	64.3689	310.465	11.0478	1.00131
%_6	Qgau	329.535	x	x	x	134.521	329.535	5.17991	1.46258
%_9	Qgau	408.326	x	x	x	100.565	408.326	5.17166	1.13365
%_22	Qgau	416.833	x	x	x	87.2812	416.833	4.36496	1.52107

%_12	Qgau	457.493	x	x	x	65.9744	457.493	10.7983	1.29203
%_2	Qgau	479.585	x	x	x	748.333	479.585	5.66739	1.59519
%_18	Qgau	493.135	x	x	x	53.6515	493.135	6.42061	1.0154
%_1	Qgau	507.86	x	x	x	1094.59	507.86	5.89464	1.43703
%_10	Qgau	762.793	x	x	x	81.8443	762.793	5.87048	1.46563
%_11	Qgau	977.937	x	x	x	54.0813	977.937	10.7255	1.67363
%_15	Qgau	1038.88	x	x	x	53.502	1038.88	28.1214	1.79219
%_8	Qgau	1100.06	x	x	x	113.809	1100.06	18.1919	0.999891
%_43	Qgau	1285.51	x	x	x	147.035	1285.51	16.5655	1.005
%_44	Qgau	1246.86	x	x	x	87.4235	1246.86	9.92953	1.00566
%_5	Qgau	1261.93	x	x	x	168.032	1261.93	15.3376	1.00806
%_17	Qgau	1312.71	x	x	x	89.3557	1312.71	25.1577	1.00903
%_45	Qgau	1319.28	x	x	x	53.4234	1319.28	16.7163	1.21948
%_20	Qgau	1385.7	x	x	x	112.394	1385.7	37.5886	1.00826
%_7	Qgau	1449.97	x	x	x	125.125	1449.97	22.2795	1.00664

Albite X050007 (Raman, unoriented, 785)

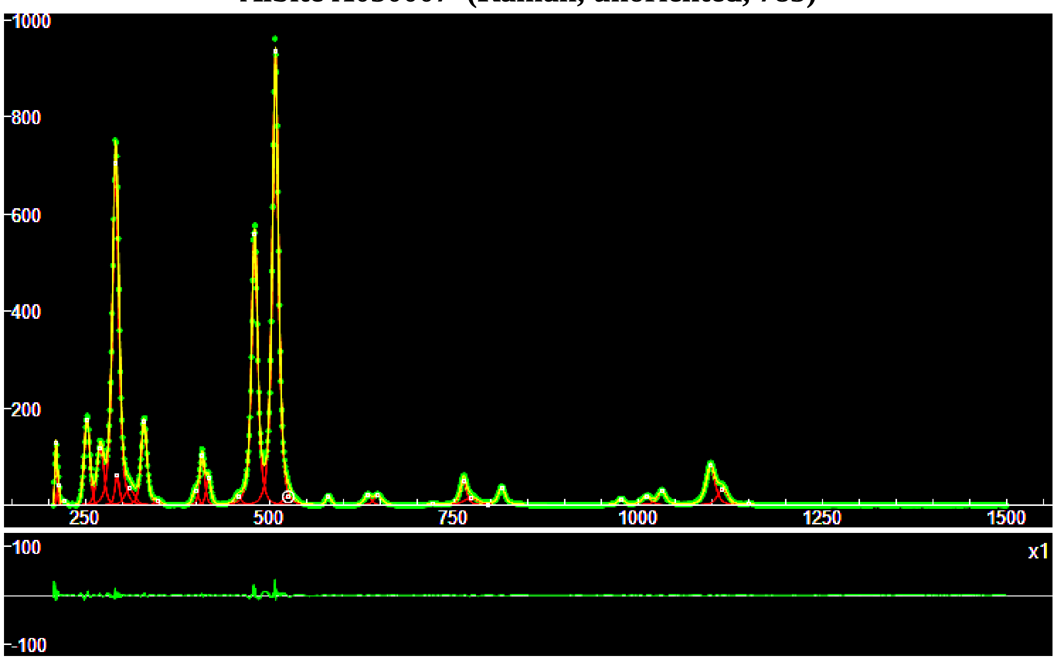

#	PeakType	Center				Height(H>20)	Center	HWHM	q-parameters...
%_6	Qgau	209.693	x	x	x	128.352	209.693	1.9067	1.00285
%_35	Qgau	212.822	x	x	x	45.3626	212.822	2.19071	1.06264
%_4	Qgau	251.785	x	x	x	175.698	251.785	5.27903	1.12791
%_8	Qgau	269.966	x	x	x	119.26	269.966	6.12472	1.3683
%_2	Qgau	290.58	x	x	x	703.918	290.58	5.44008	1.54349
%_19	Qgau	292.728	x	x	x	62.0563	292.728	3.5875	1.61197
%_12	Qgau	309.766	x	x	x	34.0411	309.766	9.0712	1.27691
%_5	Qgau	329.302	x	x	x	174.952	329.302	4.8613	1.53112
%_33	Qgau	399.211	x	x	x	28.5382	399.211	5.81482	1.0619

%_7	Qgau	408.223	x	x	x	103.684	408.223	3.99086	1.47371
%_21	Qgau	416.788	x	x	x	57.214	416.788	3.92679	1.49897
%_3	Qgau	479.449	x	x	x	562.494	479.449	5.07745	1.61385
%_1	Qgau	507.641	x	x	x	937.822	507.641	5.12462	1.57318
%_14	Qgau	646.753	x	x	x	21.4629	646.753	7.38178	1.35614
%_10	Qgau	762.931	x	x	x	51.9975	762.931	5.04957	1.69599
%_11	Qgau	814.66	x	x	x	36.6884	814.66	5.77743	1.84211
%_13	Qgau	1032.19	x	x	x	29.5902	1032.19	6.89011	1.79892
%_9	Qgau	1098.31	x	x	x	81.8333	1098.31	7.44286	1.63915
%_23	Qgau	1114.25	x	x	x	33.0962	1114.25	8.88871	1.48534

Peak positions ALBITE

Here we consider the peaks positions of some cases given above. We report on the cases where the measured chemistry is given by RRUFF database. Raman shifts have been rounded.

Albite R040068 (Raman, depolarized) $(Na_{0.99}Ca_{0.01})Al_{1.00}(Si_{0.99}Al_{0.01})_3O_8$
147 163 185 208 251 268 290 296 328 405 416 456 478 507 578 763 814 1032 1100

Albite R040129 (Raman, depolarized) $(Na_{0.99}K_{0.01})Al_{1.00}Si_{3.00}O_8$
113 149 169 186 208 251 269 290 328 416 456 478 507 579 763 775 815 1009 1099 1115

Albite R050253 (Raman, depolarized) $(Na_{0.99}Ca_{0.01})Al_{1.00}(Si_{0.99}Al_{0.01})_3O_8$
112 149 165 183 208 268 290 327 414 456 469 478 506 524 577 762 771 814 1010 1099 1116

Albite R050402 (Raman, depolarized) $Na_{1.00}Al_{1.00}Si_{3.00}O_8$
166 186 206 212 272 284 293 331 353 458 471 480 500 509 582 600 626 649 764 813 857 978 1004 1102 1270 1121 1454

Albite R230008 (Raman, depolarized, 532) $Na_{0.994}K_{0.0010}Ca_{0.0033}Sr_{0.0009}(Al_{1.008}Si_{2.993})O_8$
114 150 162 170 186 209 271 291 305 329 409 417 458 480 508 580 644 746 764 776 804 816 835 981 1013.66 1044 1102 1118 1152

Albite R060054 (Raman, unoriented, 532) $(Na_{0.67}K_{0.18}Ca_{0.15})_{\Sigma=1}Al_{1.00}(Si_{2.85}Al_{0.15})_{\Sigma=3}O_8$
121 137 169 195 198 258 281 382 404 455 474 496 511 569 775

Albite R060054 (Raman, unoriented, 785) $(Na_{0.67}K_{0.18}Ca_{0.15})_{\Sigma=1}Al_{1.00}(Si_{2.85}Al_{0.15})_{\Sigma=3}O_8$
166 194 279 330 368 404 473 499 511 566 768 1034 1112

Albite R070268 (Raman, unoriented, 532) $Na_{0.77}Ca_{0.22}Al_{1.22}Si_{2.78}O_8$
165 174 184 195 207 266 287 329 411 456 467 479 491 496 507 523 570 764 794 809 1101

Albite R070268 (Raman, unoriented, 785) $Na_{0.77}Ca_{0.22}Al_{1.22}Si_{2.78}O_8$
175 191 205 246 262 285 400 411 456 471 479 496 508 525 571 764 799 809 816 1036 1049 1081 1097 1103 1112

Albite R100169 (Raman, unoriented, 532)
147 162 172 176 185 200 209 244 252 271 283 291 312 329 400 408 417 470 479 497 507 509 521 640 756 764 775 814 1014 1032 1099 1117

Albite R100169 (Raman, unoriented, 780)
111 145 153 161 171 184 198 208 251 271 283 290 328 399 407 416 464 478 494 506 508 762 814 1032 1098

ATR-IR fingerprints

Albite R040068 Infrared

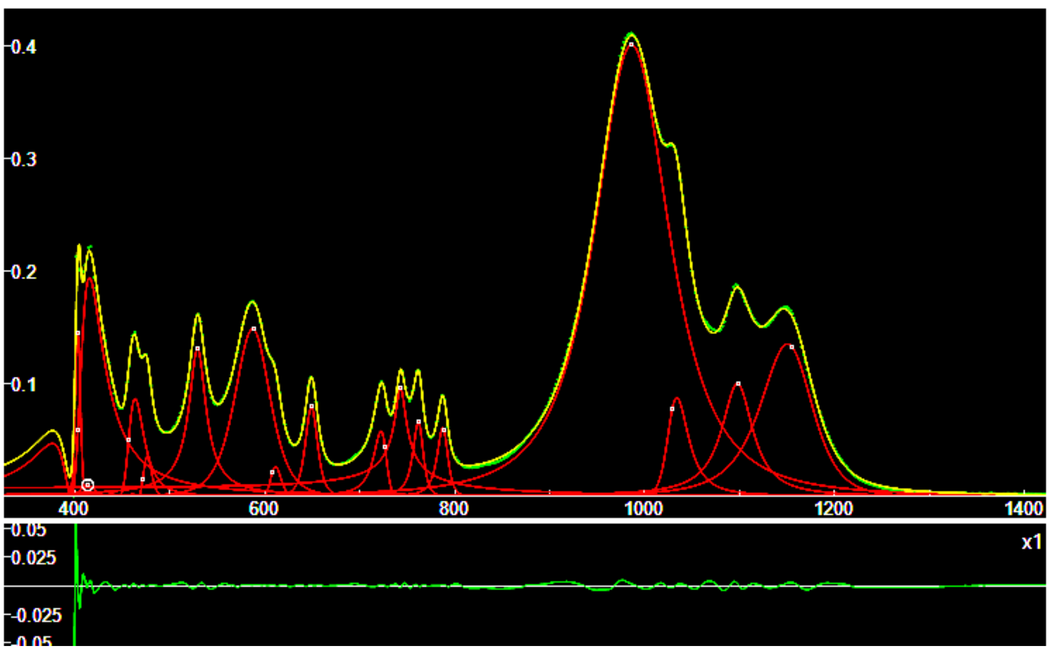

The deconvolution shown in the screenshot given above is obtained by means of q-BWF functions, which are asymmetric functions. Note that the center of the q-BWF functions (the white dot) does not coincide with the peak of the function. We can observe a few very asymmetric cases. Let us compare this deconvolution with the following one, obtained with q-Gaussian (symmetric) functions.

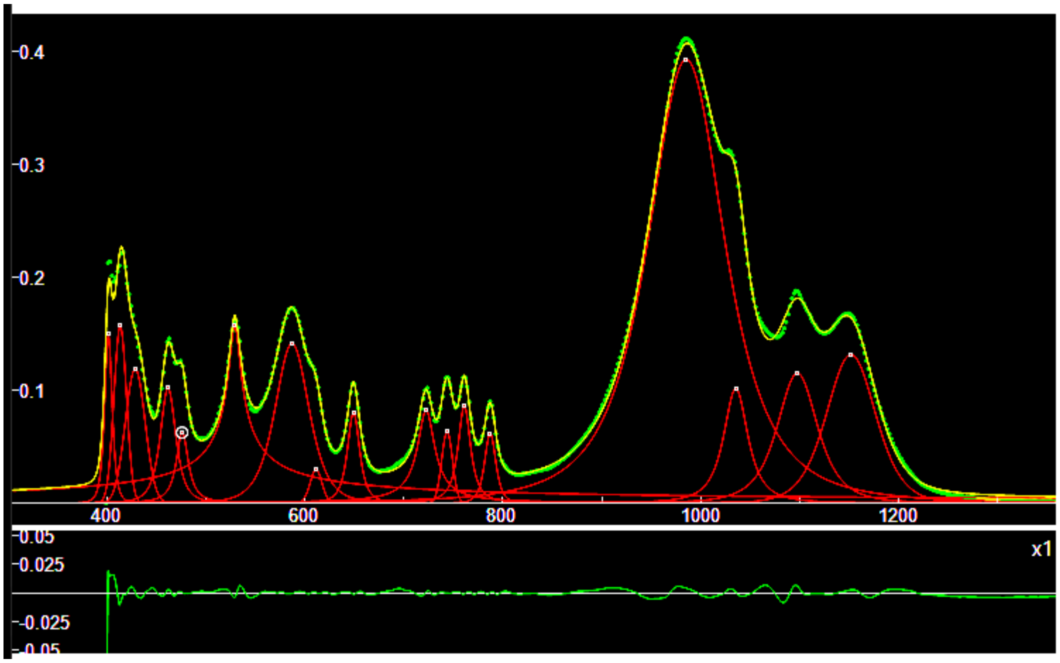

The deconvolution obtained with q-Gaussian functions is showing a larger misfit, but it is able of providing easily the positions of the peaks. For the sake of simplicity, here we propose only the ATR-IR fingerprints coming from the use of the q-Gaussian functions.

# PeakType		Center				Height Center HWHM q-parameters...
%_36	Qgau	401.49	x	x	x	0.1498 401.49 4.92 1.5
%_28	Qgau	413.481	x	x	x	0.157097 413.481 8.92973 0.999994
%_34	Qgau	428.636	x	x	x	0.118874 428.636 14.1485 0.999986
%_35	Qgau	461.768	x	x	x	0.102068 461.768 9.96172 1.61791
%_39	Qgau	476.167	x	x	x	0.0630787 476.167 7.34084 1.92729
%_32	Qgau	529.138	x	x	x	0.157738 529.138 9.19606 3.7942
%_25	Qgau	587.025	x	x	x	0.1413 587.025 22.5322 1.40359
%_27	Qgau	611.246	x	x	x	0.0301547 611.246 8.17935 1.11613
%_24	Qgau	649.095	x	x	x	0.080517 649.095 7.78329 1.67746
%_1	Qgau	985.172	x	x	x	0.392214 985.172 49.61 1.6099
%_21	Qgau	722.421	x	x	x	0.082241 722.421 10.5252 2.27941
%_20	Qgau	743.62	x	x	x	0.0633633 743.62 7.7492 0.999995
%_22	Qgau	761.007	x	x	x	0.0863925 761.007 7.7154 1.85403
%_23	Qgau	787.154	x	x	x	0.0620445 787.154 7.29431 1.51331
%_8	Qgau	1035.19	x	x	x	0.101511 1035.19 15.2067 1.76723
%_18	Qgau	1097.43	x	x	x	0.115088 1097.43 26.1931 1.56274
%_19	Qgau	1151.57	x	x	x	0.1314 1151.57 33.6226 1.27363

Albite R040129 Infrared

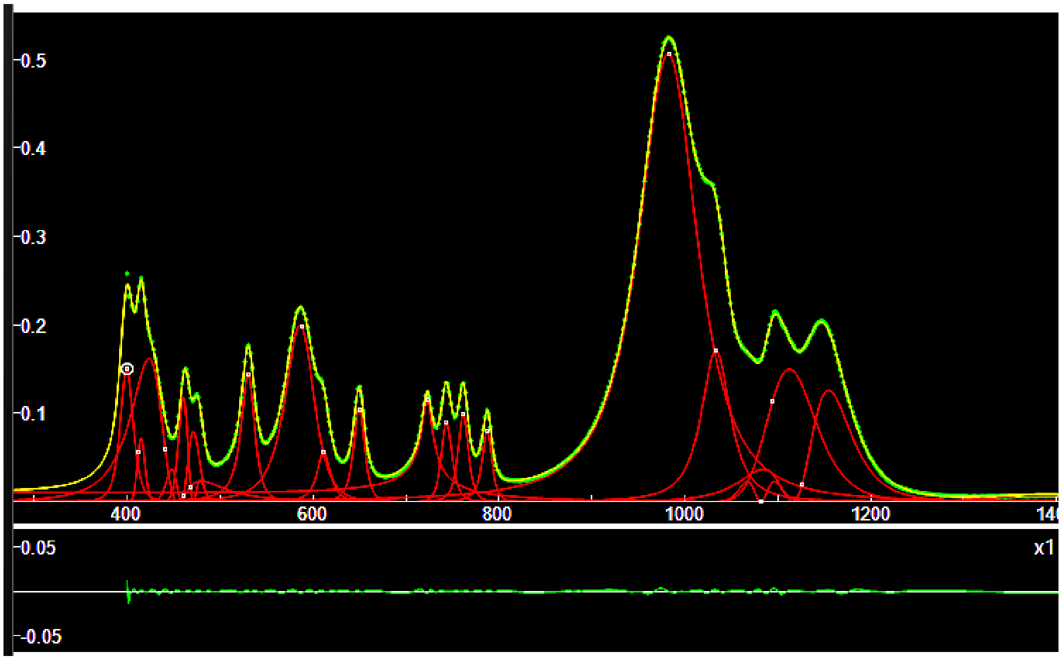

Deconvolution obtained with q-BWF functions

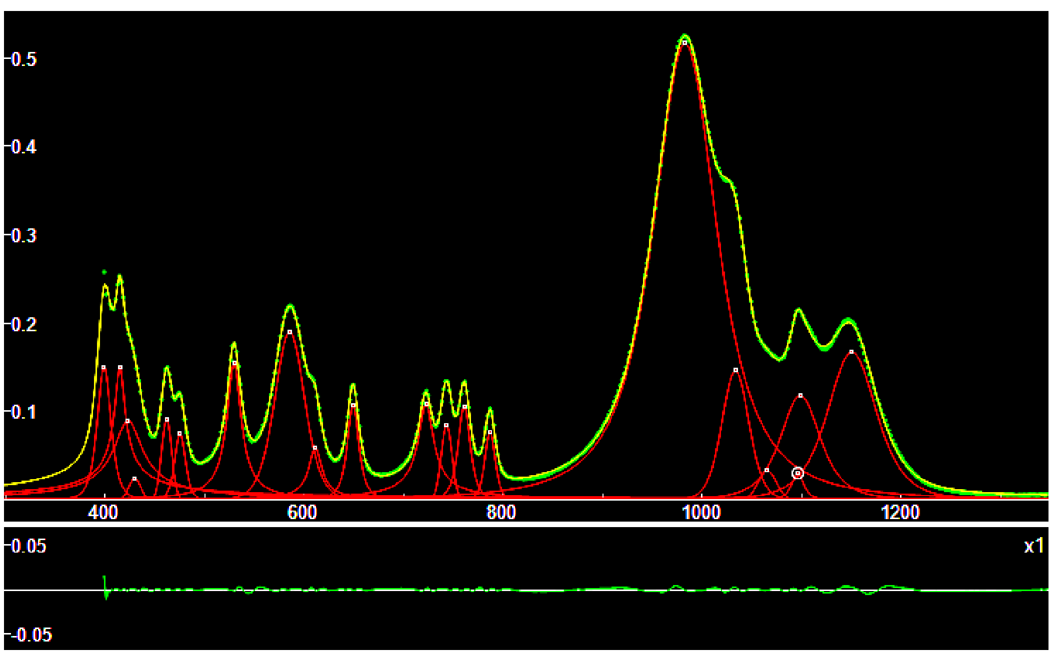

Deconvolution obtained with q-Gaussian functions

# PeakType		Center				Height	Center	Area HWHM	q-parameter
%_8	Qgau	399.2	x	x	x	0.1512	399.2	8.9	1.5
%_28	Qgau	414.951	x	x	x	0.151059	414.951	6.6402	3.29839
%_30	Qgau	423.285	x	x	x	0.0900582	423.285	18.0401	2.5924
%_3	Qgau	429.916	x	x	x	0.0244748	429.916	8.39258	0.999995
%_29	Qgau	462.019	x	x	x	0.0919753	462.019	7.1498	1.00466
%_27	Qgau	475.576	x	x	x	0.0757159	475.576	7.1059	1.35698
%_31	Qgau	529.764	x	x	x	0.155113	529.764	8.67363	2.20247
%_25	Qgau	585.752	x	x	x	0.190132	585.752	20.4907	1.23364
%_24	Qgau	611.494	x	x	x	0.0596435	611.494	7.82904	2.35488
%_26	Qgau	649.403	x	x	x	0.107495	649.403	7.30225	1.69804
%_33	Qgau	722.64	x	x	x	0.108569	722.64	9.58095	2.53109
%_34	Qgau	743.391	x	x	x	0.0847492	743.391	7.6037	1.00001
%_35	Qgau	761.057	x	x	x	0.10629	761.057	7.78834	1.56695
%_32	Qgau	787.056	x	x	x	0.0771867	787.056	6.85163	1.38785
%_13	Qgau	982.945	x	x	x	0.51629	982.945	40.8413	1.69871
%_14	Qgau	1033.68	x	x	x	0.14615	1033.68	18.5837	1.19292
%_23	Qgau	1065.67	x	x	x	0.033151	1065.67	12.9585	0.999988
%_4	Qgau	1096.26	x	x	x	0.0303404	1096.26	7.72286	1.60869
%_15	Qgau	1098.87	x	x	x	0.118282	1098.87	25.9827	1.53962
%_16	Qgau	1150.81	x	x	x	0.167191	1150.81	32.4568	1.43304

Albite R050253 Infrared

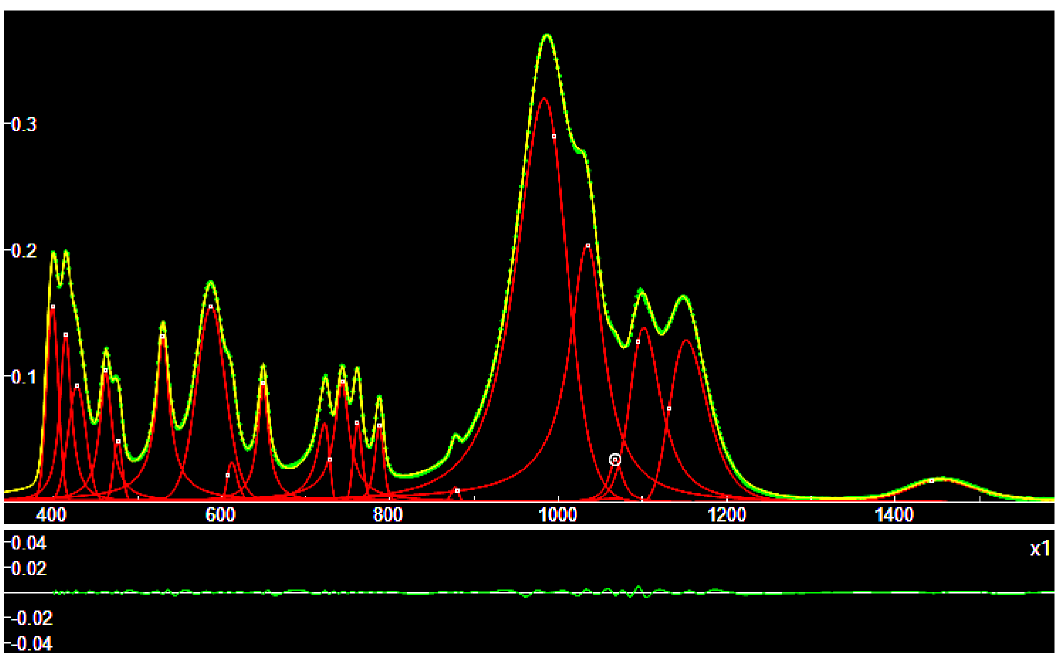

Deconvolution with q-BWF functions

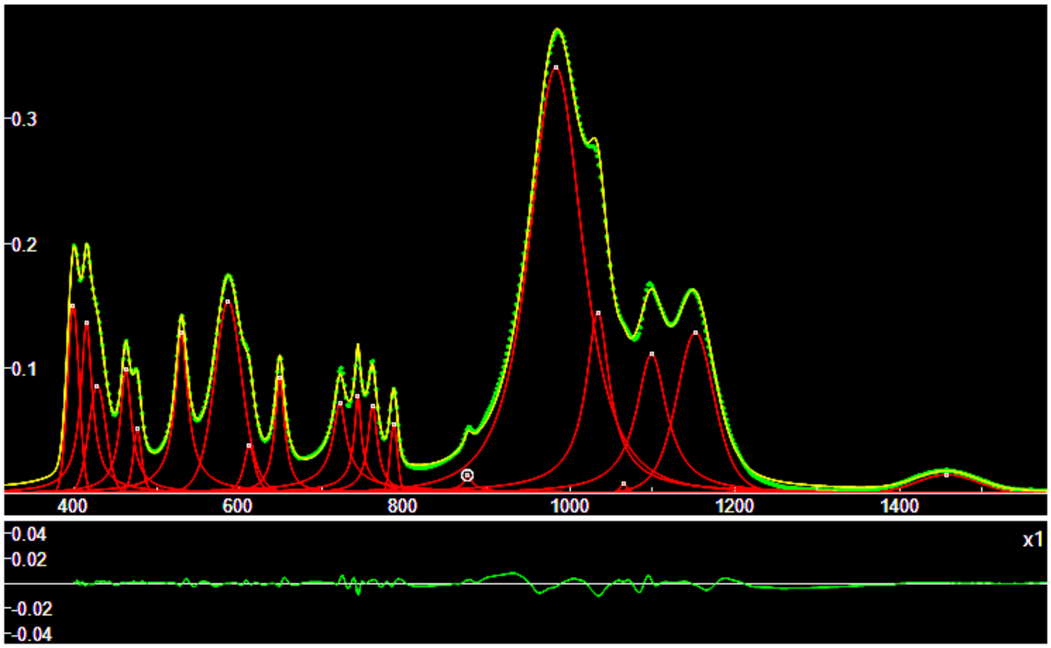

Deconvolution with q-Gaussian functions

# PeakType		Center			Height	Center	HWHM	q-parameter
%_25	Qgau	398.52	x	x	x	0.150741	398.52	9.86995 1.03197
%_24	Qgau	414.626	x	x	x	0.137107	414.626	8.03362 2.30151
%_23	Qgau	427.737	x	x	x	0.0863886	427.737	14.7006 1.085
%_22	Qgau	462.289	x	x	x	0.0996339	462.289	8.06911 2.29329
%_33	Qgau	476.269	x	x	x	0.0513655	476.269	6.6174 1.46107
%_31	Qgau	529.758	x	x	x	0.128992	529.758	8.99568 2.38356
%_30	Qgau	586.314	x	x	x	0.153904	586.314	22.4572 1.24615
%_29	Qgau	611.977	x	x	x	0.0385766	611.977	8.1429 1.81917
%_27	Qgau	648.841	x	x	x	0.0923015	648.841	7.18548 2.1242
%_26	Qgau	721.552	x	x	x	0.0728433	721.552	9.52837 2.85526
%_21	Qgau	743.442	x	x	x	0.0791623	743.442	4.78084 2.90215
%_20	Qgau	761.233	x	x	x	0.0706259	761.233	6.99555 2.26858
%_19	Qgau	786.923	x	x	x	0.0551851	786.923	6.23997 1.08324
%_1	Qgau	876.91	x	x	x	0.0150946	876.91	5.67335 3.47593
%_16	Qgau	983.283	x	x	x	0.340397	983.283	41.26 1.6072
%_14	Qgau	1034.21	x	x	x	0.145075	1034.21	17.0786 2.33946
%_4	Qgau	1065.6	x	x	x	0.0079	1065.6	5.80276 1.5
%_7	Qgau	1099.29	x	x	x	0.11138	1099.29	22.4024 2.0667
%_6	Qgau	1152.42	x	x	x	0.12886	1152.42	30.4477 1.33153
%_2	Qgau	1457.31	x	x	x	0.0151314	1457.31	52.7996 1.00786

Albite R050402 Infrared

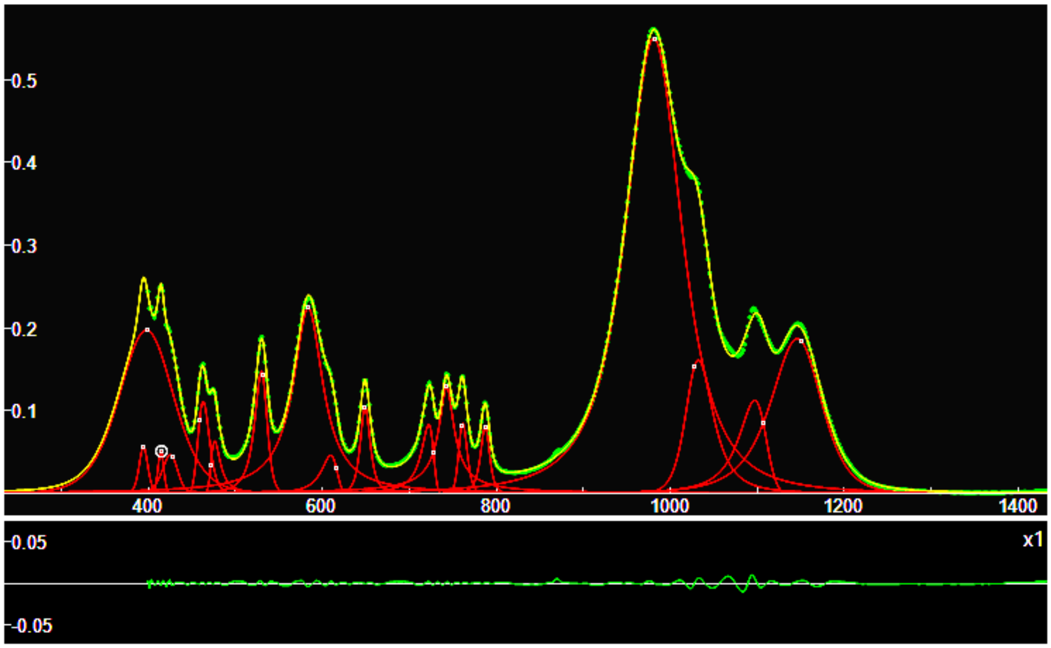

Deconvolution with q-BWF functions

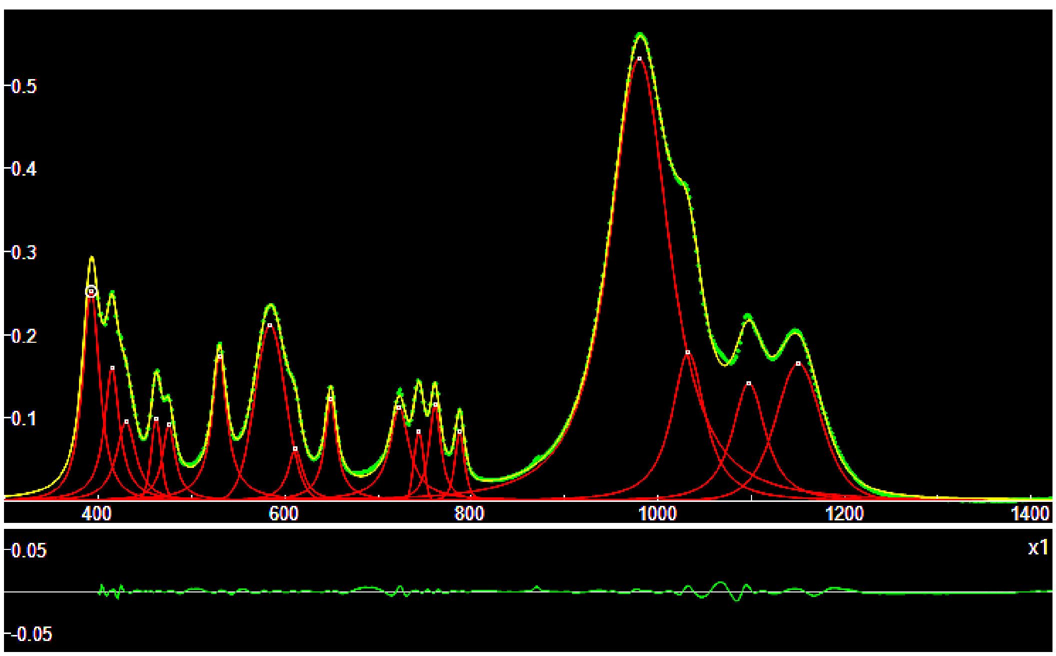

Deconvolution with q-Gaussian functions

#	PeakType	Center	Height	Center	HWHM	q-parameters
%_34	Qgau	391.955	x	x	x	0.252503 391.955 11.3729 1.79324
%_32	Qgau	414.257	x	x	x	0.16102 414.257 9.5958 2.09562
%_31	Qgau	429.487	x	x	x	0.0955367 429.487 12.905 1.93933

%_20	Qgau 461.635	x	x	x	0.0983941 461.635 7.2113 1.31996
%_21	Qgau 475.303	x	x	x	0.0916724 475.303 8.17434 2.15805
%_22	Qgau 529.676	x	x	x	0.175327 529.676 9.4696 2.18013
%_23	Qgau 584.019	x	x	x	0.211893 584.019 22.7819 1.09484
%_24	Qgau 611.124	x	x	x	0.0623193 611.124 9.55742 2.08476
%_25	Qgau 649.097	x	x	x	0.122601 649.097 7.55204 2.23
%_26	Qgau 722.522	x	x	x	0.113063 722.522 12.2366 2.22749
%_27	Qgau 743.443	x	x	x	0.0836941 743.443 7.29324 0.999995
%_28	Qgau 760.709	x	x	x	0.11652 760.709 7.55333 1.9766
%_29	Qgau 787.255	x	x	x	0.0827796 787.255 6.4593 1.62137
%_19	Qgau 979.879	x	x	x	0.532015 979.879 39.9466 1.72111
%_18	Qgau 1032.58	x	x	x	0.178682 1032.58 21.7788 1.87537
%_10	Qgau 1097.37	x	x	x	0.142287 1097.37 21.993 1.80083
%_17	Qgau 1150.45	x	x	x	0.165922 1150.45 32.5804 1.35236

Peaks positions

Albite R040068 Infrared

401 413 429 462 476 529 587 611 649 722 744 761 787 985 1035 1097 1152

Albite R040129 Infrared

399 415 423 430 462 476 530 586 611 649 723 744 761 787 983 1034 1066 1096 1099 1151

Albite R050253 Infrared

399 415 428 462 476 530 586 612 649 722 743 761 787 877 983 1034 1066 1100 1152 1457

Albite R050402 Infrared

392 414 429 462 475 530 584 611 649 723 743 761 787 980 1033 1097 1150

Raman and Infrared spectra for comparison

Albite R040068

Raman: 147 163 185 208 251 268 290 296 328 405 416 456 478 507 578 763 814 1032 1100 **Infrared:** 401 413 429 462 476 529 587 611 649 722 744 761 787 985 1035 1097 1152

Albite R040129

Raman: 113 149 169 186 208 251 269 290 328 416 456 478 507 579 763 775 815 1009 1099 1115 **Infrared:** 399 415 423 430 462 476 530 586 611 649 723 744 761 787 983 1034 1066 1096 1099 1151

Albite R050253
Raman: 112 149 165 183 208 268 290 327 414 456 469 478 506 524 577 762 771 814 1010 1099 1116 **Infrared**: 399 415 428 462 476 530 586 612 649 722 743 761 787 877 983 1034 1066 1100 1152 1457

Albite R050402
Raman: 166 186 206 212 272 284 293 331 353 458 471 480 500 509 582 600 626 649 764 813 857 978 1004 1102 1270 1121 1454 **Infrared**: 392 414 429 462 475 530 584 611 649 723 743 761 787 980 1033 1097 1150

Discussion
In Befus et al., 2018, we can find the Raman shift of Albite, under the effect of pressure. In their Supplementary material, the authors, Befus and coworkers, are providing the data of the peaks marked in their Figure 2 (cm^{-1}):

162 171 186 210 291 329 479 508 584 764 814 **881** 1033 1095 1160

Let us compare with the fingerprints given above, for the components with positions close to the Befus et al.'s values (if possible):

Befus et al.	162	171	186	210	291	329	479	508	584	764	814	1033	1095
R040068:		169	186	208	290	328	478	507	579	763	815		1099
R040129		169	186	208	290	328	478	507	579	763	815		1099
R050253:		165	183	208	290	327	478	506	577	762	814		1099
R050402:		166	186	206	293	331	480	509	582	764	813		1102
R230008:		170	186	209	291	329	480	508	580	764	816		
R100169:		172	185	209	291	329	479	507 509		764	814	1032	1099
R100169:	161	171	184	208	290	328	478	508		762	814	1032	1098
R070268:		165	184	207	287	329	479	507		764	809		1101
R070268:		175	191	205			479	508		764	816	1036	1097 1103
R060054		169	195		281		474	511	569	775			
R060054		166	194			330	473	511	566	768		1034	1112

The fingerprint given above are characterized by the following measured chemical compositions: R040068 $(Na_{0.99}Ca_{0.01})Al_{1.00}(Si_{0.99}Al_{0.01})_3O_8$, R040129 $(Na_{0.99}K_{0.01})Al_{1.00}Si_{3.00}O_8$, R050253 $(Na_{0.99}Ca_{0.01})Al_{1.00}(Si_{0.99}Al_{0.01})_3O_8$, R230008 $Na_{0.994}K_{0.0010}Ca_{0.0033}Sr_{0.0009}(Al_{1.008}Si_{2.993})O_8$. The case R050402 is given with the ideal chemistry $Na_{1.00}Al_{1.00}Si_{3.00}O_8$. And R100169 is proposed without any information about measured chemistry.
R070268 has a measured chemistry given as $Na_{0.77}Ca_{0.22}Al_{1.22}Si_{2.78}O_8$ and R060054 $(Na_{0.67}K_{0.18}Ca_{0.15})_{\Sigma=1}Al_{1.00}(Si_{2.85}Al_{0.15})_{\Sigma=3}O_8$.
Note the absence, in the fingerprints given above, of the peak at 881 cm^{-1}, which is present in data from Belus et al., 2018. This is a band of ethanol used during the measurements under pressure.

References

1. Aliatis, I., Lambruschi, E., Mantovani, L., Bersani, D., Andò, S., Diego Gatta, G., Gentile, P., Salvioli-Mariani, E., Prencipe, M., Tribaudino, M., & Lottici, P.P. (2015). A comparison between ab initio calculated and measured Raman spectrum of triclinic albite (NaAlSi3O8). Journal of Raman Spectroscopy, 46(5), pp.501-508.
2. Befus, K. S., Lin, J. F., Cisneros, M., & Fu, S. (2018). Feldspar Raman shift and application as a magmatic thermobarometer. American Mineralogist, 103(4), 600-609.
3. Bornioli, R., Fadda, S., Fiori, M., Grillo, S. M., & Marini, C. (1996). Genetic aspects of albite deposits from central Sardinia: mineralogical and geochemical evidence. Exploration and Mining Geology, 1(5), 61-72.
4. Couty, R., & Velde, B. (1986). Pressure-induced band splitting in infrared spectra of sanidine and albite. American Mineralogist, 71(1-2), 99-104.
5. D'Ippolito, V., Andreozzi, G. B., Bersani, D., & Lottici, P. P. (2015). Raman fingerprint of chromate, aluminate and ferrite spinels. Journal of Raman Spectroscopy, 46(12), 1255-1264.
6. Dondi, M., Guarini, G., Conte, S., Molinari, C., Soldati, R., & Zanelli, C. (2019). Deposits, composition and technological behavior of fluxes for ceramic tiles. Periodico di Mineralogia, 88(3).
7. Dondi, M., Conte, S., Molinari, C., & Zanelli, C. (2025). Mineral Resources for the Ceramic Industry: Survey of Feldspathic Raw Materials in Italy. Minerals, 15(1), 87.
8. Fenske, M. R., Braun, W. G., Wiegand, R. V., Quiggle, D., McCormick, R., & Rank, D. H. (1947). Raman spectra of hydrocarbons. Analytical Chemistry, 19(10), 700-765.
9. Freeman, J. J., Wang, A., Kuebler, K. E., Jolliff, B. L., & Haskin, L. A. (2008). Characterization of natural feldspars by Raman spectroscopy for future planetary exploration. The Canadian Mineralogist, 46(6), 1477-1500.
10. Fuertes, V., Cabrera, M. J., Seores, J., Muñoz, D., Fernández, J. F., & Enríquez, E. (2018). Hierarchical micro-nanostructured albite-based glass-ceramic for high dielectric strength insulators. Journal of the European Ceramic Society, 38(7), 2759-2766.
11. Fuertes, V., Reinosa, J. J., Fernández, J. F., & Enríquez, E. (2022). Engineered feldspar-based ceramics: A review of their potential in ceramic industry. Journal of the European Ceramic Society, 42(2), 307-326.
12. Hanel, R., Thurner, S., & Tsallis, C. (2009). Limit distributions of scale-invariant probabilistic models of correlated random variables with the q-Gaussian as an explicit example. The European Physical Journal B, 72(2), 263.
13. Johnson, E. A., & Rossman, G. R. (2003). The concentration and speciation of hydrogen in feldspars using FTIR and 1H MAS NMR spectroscopy. American Mineralogist, 88(5-6), 901-911.
14. Jovanovski, G., & Makreski, P. (2016). Minerals from Macedonia. XXX. Complementary use of vibrational spectroscopy and X-ray powder diffraction for spectra-structural study of some cyclo-, phyllo-and tectosilicate minerals. A review. Macedonian Journal of Chemistry and Chemical Engineering, 35(2), 125–155.
15. Lafuente, B., Downs, R. T., Yang, H., & Stone, N. (2015). 1. The power of databases: The RRUFF project. In Highlights in mineralogical crystallography (pp. 1-30). De Gruyter (O).
16. McKeown, D. A. (2005). Raman spectroscopy and vibrational analyses of albite: From 25 C through the melting temperature. American Mineralogist, 90(10), 1506-1517.

17. Moenke, H. (1962) Mineralspektren. I. Akademie-Verlag, Berlin.
18. Moenke, H. (1966) Mineralspektren. II. Akademie-Verlag, Berlin.
19. Mooney, J. F. (1996). Ceramics & glass. In Industrial Minerals and Their Uses (pp. 459-481). William Andrew Publishing.
20. Palomba, M. (2001). Geological, mineralogical, geochemical features and genesis of the albitite deposits of Central Sardinia (Italy). Guidebook to the field trips in Sardinia of the WRI, 10, 35-57.
21. Russo, M., Punzo, I., Blass, G., & Ciriotti, M. E. (2007). Zirconolite, Albite ed epidoto: nuova e poco note specie del Somma-Vesuvio. Micro (UK report), 43-48.
22. Salje, E., Güttler, B., & Ormerod, C. (1989). Determination of the degree of Al, Si order Q od in kinetically disordered albite using hard mode infrared spectroscopy. Physics and Chemistry of Minerals, 16, 576-581.
23. Smith, J. V., Artioli, G., & Kvick, A. (1986). Low albite, NaAlSi3O8: Neutron diffraction study of crystal structure at 13 K. American Mineralogist, 71(5-6), 727-733.
24. Sparavigna, A. C. (2023). SERS Spectral Bands of L-Cysteine, Cysteamine and Homocysteine Fitted by Tsallis q-Gaussian Functions. International Journal of Sciences, 12(09), 14-24.
25. Sparavigna, A. C. (2023). q-Gaussian Tsallis Line Shapes and Raman Spectral Bands. International Journal of Sciences, 12(03), 27-40.
26. Sparavigna, A. C. (2023). q-Gaussian Tsallis Line Shapes for Raman Spectroscopy (June 7, 2023). SSRN Electronic Journal. DOI: 10.2139/ssrn.4445044
27. Sparavigna A. C. (2023). Tsallis q-Gaussian function as fitting lineshape for Graphite Raman bands. ChemRxiv. Cambridge: Cambridge Open Engage; 2023.
28. Sparavigna, A. C. (2023). Asymmetric q-Gaussian functions generalizing the Breit-Wigner-Fano functions. Zenodo. https://doi.org/10.5281/zenodo.8356165
29. Sparavigna, A. C. (2024). Raman and Attenuated Total Reflectance Infrared RRUFF Spectra: some cases of deconvolution with q-Gaussians and q-BWF functions. SSRN Electronic Journal, DOI: 10.2139/ssrn.4993668
30. Sparavigna, A. C. (2024). Atlas of Metabolite SERS Fingerprints obtained by means of q-Gaussian deconvolutions and Fityk Software. ChemRxiv. DOI: 10.26434/chemrxiv-2024-85l19-v2
31. Sparavigna, Amelia Carolina (2025), "Albite Feldspar Mineral Raman and ATR-IR Fingerprints in Fityk .fit and .peaks files", Mendeley Data, V1, doi: 10.17632/74b2fw4fw4.1
32. Tribaudino, M., Gatta, G. D., Aliatis, I., Bersani, D., & Lottici, P. P. (2018). Al—Si ordering in albite: A combined single-crystal X-ray diffraction and Raman spectroscopy study. Journal of Raman Spectroscopy, 49(12), 2028-2035.
33. Tsallis, C. (1988). Possible generalization of Boltzmann-Gibbs statistics. Journal of statistical physics, 52, 479-487.
34. Tuttle, O. F., & Bowen, N. L. (1950). High-temperature albite and contiguous feldspars. The Journal of Geology, 58(5), 572-583.
35. von Stengel, M.O. (1977) Normal Schwingungen von Alkalifeldspäten. Zeitschrift für Kristallographie, 146, l-l8.
36. Wojdyr, M. (2010). Fityk: a general-purpose peak fitting program. Journal of applied crystallography, 43(5), 1126-1128.

37. Zhang, M., Wruck, B., Barber, A. G., Salje, E. K. H., & Carpenter, M. A. (1996). Phonon spectra of alkali feldspars: phase transitions and solid solutions. American Mineralogist, 81(1-2), 92-104.